Estimation of Intensity Duration Frequency Curves
for Current and Future Climates

By

Nicolas Desramaut

Department of Civil Engineering and Applied Mechanics

McGill University

Montreal, Quebec, Canada

June 2008

Acknowledgement

I would like to kindly and very sincerely thank my supervisor, Professor Van-Thanh-Van Nguyen, for his never-ending help, his indefectible encouragements, and his professional guidance.

I would also thank Dr Tan-Danh Nguyen and Sébastien Gagnon for their assistance in my research work, Gilles Rivard and Pierre Dupuis, for their help using the softwares, the occupants of the room 391 (Reena, Ali, Arden, Damien, John, Nabil, Reza, Salman) for their friendship and their permanent support, with a special mention to Arden, who helped me submitting this thesis despite the ocean.

And last but not least, I would like to express my deeper thanks to my family, who despite the distance, were always on my side during my stay in Montreal.

Abstract

Climate variability and change are expected to have important impacts on the hydrologic cycle at different temporal and spatial scales In order to build long-lasting drainage systems, civil engineers and urban planners should take into account these potential impacts in their hydrological simulations. However, even if Global Climate Models (GCM) are able to describe the large-scale features of the climate reasonably well, their coarse spatial and temporal resolutions prevent their outputs from being used directly in impact assessment models at regional or local scales.

This study proposes a statistical downscaling approach, based on the scale invariance concept, to incorporate GCM outputs in the derivation of Intensity-Duration-Frequency (IDF) curves and the estimation of urban design storms for current and future climates under different climate change scenarios. The estimated design storms were then used in the estimations of runoff peaks and volumes for urban watersheds of different shapes and different levels of surface imperviousness using the popular Storm Water Management Model (SWMM). Finally, a regional analysis was performed to estimate the scaling parameters of extreme rainfall processes for locations with limited or without data. In summary, results of an illustrative application of the proposed statistical downscaling approach using rainfall data available in Quebec (Canada) have indicated that it is feasible to estimate the IDF relations and the resulting design storms and runoff characteristics for current and future climates in consideration of GCM-based climate change scenarios. Furthermore, based on the proposed regional analysis of the scaling properties of extreme rainfalls in Singapore, it has been demonstrated that it is feasible to estimate the IDF curves for partially-gaged or ungaged sites.

Résumé

La variabilité et les changements climatiques devraient avoir des impacts considérables sur le cycle hydrologique aux différentes échelles spatio-temporelles. Afin de construire des systèmes de drainage durables, les ingénieurs se doivent de prendre en considération ses modifications probables dans leur simulation. Toutefois, si les Modèles de Circulation Globale (MCG) sont capables de reproduire raisonnablement bien les caractéristiques à grande échelle du climat, leurs résolutions sont trop grossières pour permettre une utilisation immédiate de leurs informations dans les modélisations urbaines.

Cette étude propose une approche de mise à l'échelle statistique, basée sur les propriétés d'invariance d'échelle, afin d'incorporer les résultats des MCG dans la conception des courbes Intensité-Durée-Fréquence (IDF) futures. Ces courbes sont ensuite utilisées pour l'estimation de l'évolution des quantités de ruissèlement. Enfin, une analyse régionale permet une évaluation des paramètres de réduction d'échelle pour des stations partiellement jaugées, voir non jaugées. C'est ainsi que des courbes IDF peuvent être construites avec un nombre limité de données.

Table of Content

List of Figures

List of Tables

1. Introduction

1.1. Context

Historically, the first urban drainage systems were built to protect the urban infrastructures from water damage. Their main task was then to convey stormwater runoff outside the city as quickly as possible. The opportunity to use these systems to dispose of wastewater appeared later, in the XIXth century, with the raising awareness of the impact of polluted water on health. Hence, the current engineering practice for the design of urban drainage systems requires taking into account these two main objectives: the removal of wastewater and the drainage of storm runoff. The first objective could be achieved by considering different wastewater treatment measures to prevent the discharge of polluted water into the receiving environment. The second objective is more difficult to address because of the random variability of runoff in time and in space due to the randomness of precipitation for current and future climates. Furthermore, the runoff process could be non-homogeneous due to expanding urbanization of the watershed causing changes in land use pattern over time (e.g., natural drainage systems such as streams have been replaced by impervious areas such as streets and residential buildings). Therefore, in addition to the effects of land use changes on the runoff process, improved estimations of precipitation patterns for current and future climates are urgently needed to provide more accurate estimation of runoff characteristics in the context of a changing climate.

Most urban drainage systems were built to last for a long time, usually more than 50 years, because their repair or retrofitting could be expensive and could cause massive disruptions of normal city activities since these systems are mainly located in underground areas. These infrastructures are designed to cope with the majority (but not all) of the extreme rainfall events that could occur during their service life (usually ranging from 50 to 100 years). In fact, in view of economic but also technical constraints, there are some limits to the capacities of drainage

1

systems. The current practice has set some criteria for the construction of drainage systems to balance construction constraints with levels of risk. The minor drainage system (piped system) should be built to be overwhelmed only every 5 to 10 years, whereas the major drainage system (overland system, including the roads and parking lots) should support nearly every event (Arisz and Burrell, 2006).

To meet the above-mentioned criteria, engineers need accurate estimations of potential runoffs from an urban watershed. However, historical runoff data are generally lacking or have become irrelevant due to changes in land use. In order to cope with this deficiency, engineers rely on conceptual urban runoff models, such as the SWMM model, to simulate the rainfall-runoff relations. Indeed, these models could describe the complex interactions between different hydrologic and hydraulic processes involved in an urban watershed to transform the input precipitation pattern into the complete output runoff hydrograph. Hence, to use these models, knowledge of current and future rainfall patterns, generally presented as standardized hyetographs, is required. This synthetic pattern of precipitation provides illustrations of probable distributions of rainfall intensity over time for a given return period at a local site. In general, these synthetic hyetographs are computed based on historic rainfall records, with the assumption that the distributions parameters are stationary or constant over time.

However, recent studies compiled in the Intergovernmental Panel on Climate Change assessment report (IPCC, 2007) have shown that extreme rainfall events are very likely to be globally more frequent and more intense in future decades. Thus, the hypothesis of stationary precipitation occurrences appears highly questionable in prospect of climate change. Hence, the design storms computed based on historic data could only be accurate for the current period but not for the whole service life of drainage systems. Consequently, to build sustainable drainage systems, engineers need to incorporate future climatic conditions into

2

their computation of design storms. The Global Climate Models (GCMs), also called General Circulation Models, are considered to be able to provide reliable scenarios for future climatic parameters at the global scale. However, their resolutions are too coarse (~300 km, 1 day) for being able to be directly used in the simulation of runoff from urban watersheds since these watersheds are normally characterized by a short response time (usually, less than 1 day) due to small surface area size and high imperviousness level. Therefore, outputs from GCMs should be downscaled to provide climate simulations at appropriate temporal and spatial scales that are required for accurate estimation of rainfall and runoff characteristics for urban watersheds.

1.2. Research Objectives

In view of the above-mentioned issues, the present study proposes a new statistical downscaling method for estimating the Intensity-Duration-Frequency (IDF) relations that could take into account the climate information given by GCMs for current as well as for future climatic conditions. More specifically, this study is aiming at the following particular objectives:

To propose a spatial-temporal statistical downscaling method to describe the linkage between daily global climate variables and local daily and sub-daily extreme rainfalls for the derivation of IDF relations for current and future climates;

To propose a procedure for constructing IDF relations for a local site that could take into account GCM-based climate change projections;

To propose a procedure for estimating the urban design storms in consideration of GCM-based climate change scenarios;

To propose a procedure for evaluating the impacts of climate change on the runoff process for urban watersheds; and to investigate the spatial variability of extreme rainfall scaling properties over a given region.

3

The first part of the study was performed assuming stationary scaling parameters for extreme rainfalls (i.e., the spatial and temporal scaling properties for future periods will be the same as the ones found for the current period). The main aim is to assess the future trends in extreme rainfall events and their consequences on design rainfalls and urban runoff properties for urban drainage system design. Notice that the hypothesis of stationary rainfall scaling parameters could only represent an approximation since these values could change due to the change in climatic conditions for future periods.

In order to deal with this stationarity issue as well as with the situations where rainfall records at the site of interest are limited or unavailable, a method is proposed in the second part to examine the spatial variability of the rainfall scaling parameters in terms of the regional variation of some climatic variables. This regional analysis could permit the estimation of IDF curves for current periods for cases with limited or without data using records from surrounding stations as well as for the estimation of IDF relations for future periods using GCM-based projections to avoid the stationarity hypothesis.

1.3. Literature Review

1.3.1. Consequences of Climate Change on Urban Drainage

During the last decades, scientists have become more and more conscious of the potential impacts of climate change on precipitation patterns for the design of urban drainage systems. Most previous studies have agreed upon the fact that, as rainfall events are likely to become more frequent and more intense, the level of services provided by the drainage systems will be reduced and these urban structures will suffer more frequent damage, reducing their service life. However, as Semadeni-Davies (2004) points out, there are neither tools nor guidelines in the

literature to assess these impacts of climate change in urban catchment areas. In view of this deficiency, this study proposes the uses of incremental scenarios, with increases of precipitation arbitrarily taken in a range of the values generated by the GCM. This method is simple and provides a range of possible consequences. However, as recognized in the study , these scenarios should not be considered as future climatic conditions, but only as a spectrum of potential impacts, as a result of the arbitrary forcing. . Watt et al. (2003) used a similar approach for estimating the evolution of the runoff values. They assumed that the rainfall intensity was increased by 15 percent. From the resulting runoff values, they estimated the parts of the drainage systems that will face overflow capacity. However, this method is based on crude estimates. They assumed that intensities of all rainfall events evolved in a similar trend, independently of their duration, with an increase directly estimated from the GCM large-scale trends. Hence, this method may not be suitable for urban catchment, where the change in precipitation patterns might be local but not uniformly proportional.

Denault et al. (2002) proposed an alternative to these methods. They determined the past linear trends of local rainfall depth for different durations ranging from 5 min to 1 day. Based on this information, and on the assumption that the linear increases remain constant, they extrapolated the future intensity-duration relationships, and, from these data, construct the corresponding design storms for future periods. They use the software SWMM (Huber and Dickinson, 2002) to perform estimations of future runoff values. This method is an alternative for assessing potential variations of design storms resulting from climate change, and therefore for evaluating hydraulic responses of catchment areas, taking into account that the shape of the design storms can be altered. However, the authors have to make the hypothesis that the increase rate of the local rainfall depth will remain the same (i.e. the increase will continue to be linear). The outputs of the GCM, usually without any persistent linear tendency, make this hypothesis highly questionable. Moreover, the recent IPCC report (IPCC, 2007) suggests that the

evolution of anthropogenic activities is very likely to have significant impacts on future climate conditions. And this evolution would certainly not be linear. So we need to take into account uncertain nonlinear future causes to assess future effects.

Thus, even if scientists and decision-makers point out the need for a clear understanding of the effects of climate change on human and social activities, there is no agreement regarding the suitable approach for evaluating its impacts on urban hydrologic processes.

1.3.2. Design Storms

Design storms have been used extensively by civil engineers to size sewers for more than 60 years. With the nonlinear interactions between rainfall and runoff processes as described by various urban runoff models, these synthetic design storms are required for the estimation of the complete runoff hydrographs for urban drainage design purposes. Many frameworks have been conceived in different countries for the computation of design storms (Marsalek and Watt, 1984), with varying shapes, storm durations, time to peak, maximum intensity and total volume of rainfall; however, none matches every situation, forcing hydrologists to perform assessment processes before using a design-storm model at a new site (Peyron, 2001). Peyron et al. (2005) proposed a procedure to systematically evaluate design storms models for specific locations. First, the targeted design storms for different return periods, based on rainfall data from local Intensity-Duration-Frequency (IDF) curves, were constructed. Then, these synthetic hyetographs were used as input in the SWMM model to obtain the respective runoff values (peak flows and volumes). Thus, the runoff properties estimated from the design storms were compared to those values obtained from observed historical storms to assess the accuracy of different design storm models. Based on this approach, the best design storm can be selected for the design of urban drainage systems.

2. Evaluation of IDF relations and runoff properties assuming stationarity in the rainfall scaling parameters

3.

3.1. Data

This section presents a description of the hydrologic and climate data used in the present study. In addition, a detailed analysis of these data is described to assess the quality as well as the suitability of the data for this study.

3.1.1. Data description

For the at-site analysis, the study site is located at the Montreal Pierre-Elliot-Trudeau international airport in Dorval, Quebec (Canada), in the west part of Montreal Island (45.28N, 73.45W) as shown in Figure 1. For calibration, verification and validation purposes observed data are required. For projection in future periods, the simulated (downscaled) rainfall data from GCMs will be used.

Figure 1: Localization of the Pierre-Elliot-Trudeau International Airport in Quebec

3.1.2. Observed data

The observed Annual Maximum Precipitation (AMP) data available at the Pierre Elliot Trudeau airport for the 1961-1990 period were used in the present study. The AMP data (representing the maximum rainfall depth fallen each year on a daily or sub-daily basis) measured in millimetres (within a precision of one-tenth of millimetres) and available for 9 durations (5, 10, 15, 30 minutes; 1, 2, 6, 12 and 24 hours) were provided by Environment Canada.

Historical storm (1961/8/25)
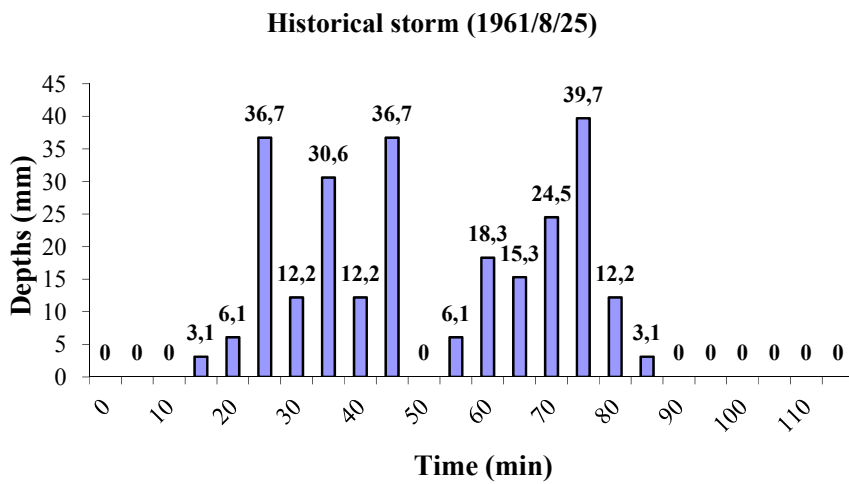
Figure 2: Example of a recorded historical storm

To investigate the accuracy of the design storm models, 140 historical rainfall events (called "storms" in the remaining of the report) were recorded during this 1961-1994 baseline period, in millimetres, with a 5-minute time step and with a one-tenth-millimetre precision. An example of a recorded storm is given in Figure 2. The selection was performed according to their ability to generate the biggest runoff events and the presence of at least one recorded storm event per year.

Year	1961	1962	1963	1964	1965	1966	1967	1968	1969
# of storms	5	2	5	2	2	4	2	1	1
Year	1970	1971	1972	1973	1974	1975	1976	1977	1978
# of storms	1	2	3	5	5	7	5	3	3
Year	1979	1980	1981	1982	1983	1984	1985	1986	1987
# of storms	1	6	3	1	2	4	1	8	8
Year	1988	1989	1990	1991	1992	1993	1994		
# of storms	4	5	11	2	3	7	16		

Table 1: Repartition of the historical storms during the 1961-1994 baseline period

3.1.3. Simulated data

Daily rainfalls for the baseline 1961-1994 period and for three 30-year future periods (2010-2039; 2040-2069; and 2070-2099) were provided by Dr. Tan-Danh Nguyen (Department of Civil Engineering and Applied Mechanics, McGill University) using the Statistical Downscaling Model (SDSM) (Wilby et al. 2002), from driven conditions from Global Climate Models (GCM) inputs (Nguyen et al., 2006). This linear regression based downscaling method allows the development of the linear statistical linkages between large-scale predictors from GCMs and local observed predictands (e.g., the daily rainfall in this study). The GCM climatic variable data are from two different GCMs:

- Hadley Centre Coupled Model, version 3 (HadCM3) (Johns et al., 2003), Hadley Centre, United Kingdom

- Coupled Global Climate Model, second generation (CGCM2), (Flato and Boer, 2001), Canadian Center for Climate modelling and analysis, Canada

These series of simulations under climate change conditions use the SRES A2 emission scenario with the hypothesis of greenhouse gases (GHG) emissions following the SRES A2 scenario (Nakicenovic et al., 2000). This scenario is based on the assumption that the world will become more and more heterogeneous, with a continuously increasing population (15 billion by 2100), slow and regional economic growths, and few inter-country technological transfers. This scenario forecasts that the level of CO_2 in the atmosphere will be double in 2100 compared with the pre-industrial concentration. In the present study, a set of 100 simulations were performed for each model and for each future period considered.

3.1.4. Bias correction for the daily precipitation simulation

According to Nguyen et al. (2006) , there is a bias between the daily AMPs obtained by the statistical downscaling results from different GCM outputs using the SDSM procedures and the observed values, as illustrated in . Hence, an bias-correction adjustment is required to improve the precision of these predictions.
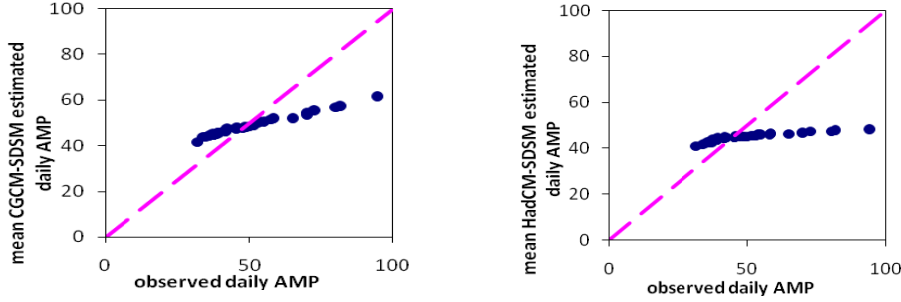
Figure 3: Difference between raw SDSM estimates and observed values for the 1961-1994 baseline period

Nguyen et al. (2006) propose this adjustment:

$$y_i = \underline{y_i} + e_i y_i$$

in which y_i is the adjusted daily AMP in year **i**, $\underline{y_i}$ the corresponding SDSM daily AMP estimate and e_i the residual associated with $\underline{y_i}$

The residual is computed based on a second order regression:

$$e_i = m0 + m1 * \underline{y_i} + m2 * \underline{y_i}^2 + \varepsilon$$

m0, **m1** and **m2** are the polynomial coefficients and ε the resulting error.
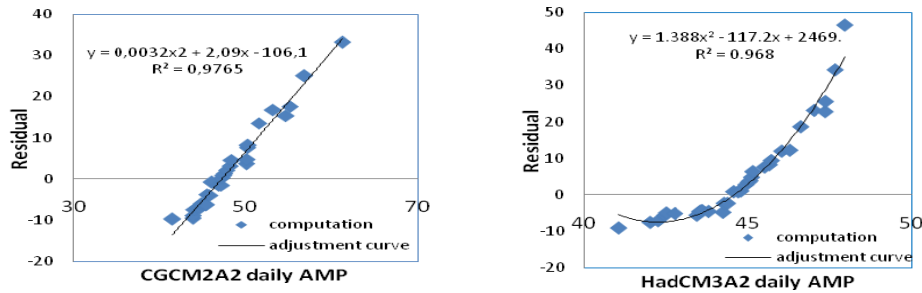
Figure 4: Adjustment functions for daily GCM downscaled AMP for the 1961-1994 baseline period.

10

This adjustment provides unbiased AMP estimations comparable with the observed annual maximum daily rainfalls (Figures 5 and 6). Indeed, the median values (the lines inside the box-plots) are quite similar with the observed ones.
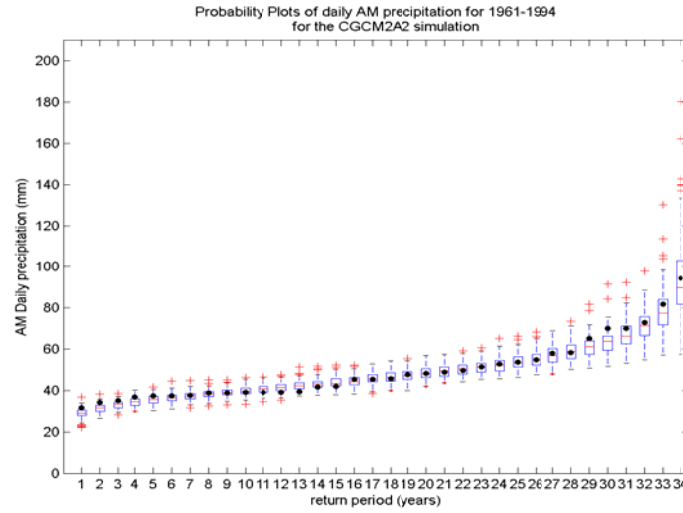
Figure 5: Box plots of the 100 adjusted AM Daily Rainfall estimations from CGCM2A2 compared with the observed values (dots), for the 1961-1994 period.
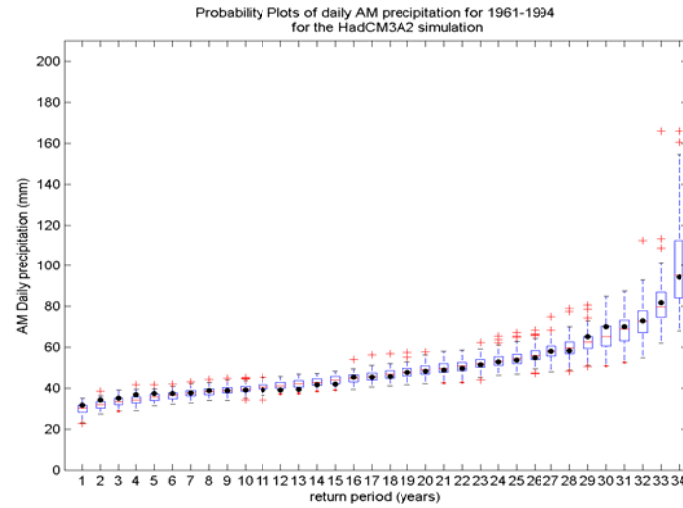
Figure 6: Box plots of the 100 adjusted AM Daily Rainfall estimations from HadCM3A2 compared with the observed values (dots), for the 1961-1994 period.

3.1.5. Selection of years with data inconsistency

In order to compare in a suitable manner the outputs of the computations with the observed data, the different sets of data have to be consistent. The maximum depths of precipitation resulting from the available recorded historical storms for 8 durations (5, 10, 15 and 30 minutes; 1, 2, 6 and 12 hours) are computed for each year, and compared with the corresponding recorded AMP (APPENDICE A). Three years (1970, 1985 and 1991) have inconsistent sets of data, as illustrated in Figure 7 with the average of the relative difference over the 8 durations. This inconsistency is due to the absence of the record of the biggest historical storm in 1970, 1985, and 1991 in our data sets. However, for these 3 years, the different values were near the median value for each duration. Hence, the removal of these data should not trigger significant bias in the simulations.
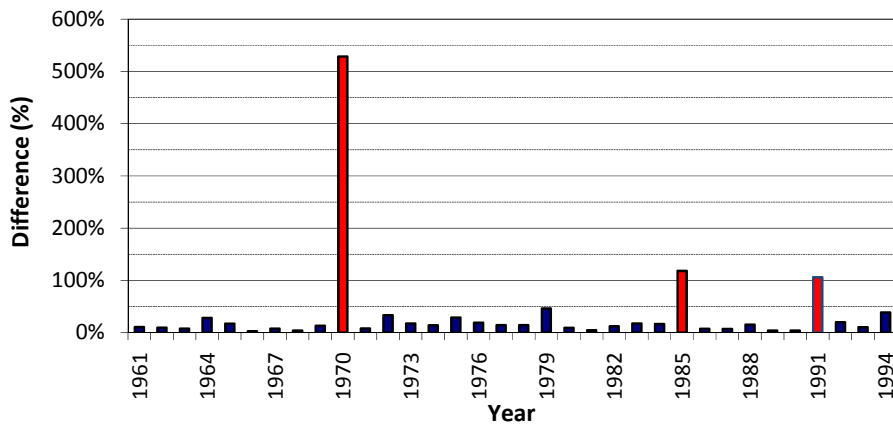
Figure 7: Difference between observed AMP and recorded historical storms

3.2. Methodology

3.2.1. Construction of IDF Curves

3.2.1.1. Generalized extreme values distribution

The General Extreme Values (GEV) distribution is a distribution commonly used to model extreme events, in particular extreme precipitations. Indeed, it has been proven to match well the observed extreme values (Nguyen et al., 1998). The GEV cumulative distribution function can be written as

$$F(X\tau; \alpha, \kappa, \xi) = exp\left(-\left(1 - \frac{\kappa}{\alpha}(X\tau - \xi)\right)^{\frac{1}{\kappa}}\right) \qquad (1)$$

where $X\tau$ is the quantile associated with a return period τ; ξ, α and κ are parameters for respectively the location, the scale and the shape.

As a result, the quantile $X\tau$ for the return period τ can be calculated as follow:

$$X_\tau = \xi + \alpha/\kappa \left[1 - (ln\,(1 - p)\,)^\wedge\kappa\,\right] \qquad (2)$$

in which p is the probability of exceedance, related to the return period:

$$p = 1/\tau \qquad (3)$$

3.2.1.2. GEV parameters estimations

The three GEV parameters are estimated by the method of the Non Central Moments (NCM), where the NCM are defined as:

$$\mu_k = E\{X^k\} \qquad (4)$$

It can be demonstrated (Nguyen et al. (2002)) that they are related to the NCM according to these equations.

$$\mu_k = \left(\xi + \frac{\alpha}{\kappa}\right)^k + (-1)^k \left(\frac{\alpha}{\kappa}\right)^k \Gamma(1 + k) + k\sum_{i=1}^{k-1}(-1)^i\left(\xi + \frac{\alpha}{\kappa}\right)^{k-i}\Gamma(1 + i\kappa) \quad (5)$$

in which $\Gamma(.)$ is the gamma function

13

Thus, using the first three NCMs ($k = 1, 2,$ and 3) given by Equation (4) the three parameters of the GEV distribution α, ξ and κ can be determined by the method of moments (see APPENDICE B)

3.2.1.3.   Empirical IDF curves

The AMPs were ranked in descending order to compute the exceedance empirical probability p_i for each rank i, using the Cunnane's plotting position formula (Cunnane, 1978):

$$p_i = \frac{i-0.4}{n+0.2} \qquad (6)$$

in which n is the number of years of the record.

 Then the return periods, assuming that there are no trends in the quantiles values (i.e., p is invariant over time), are computed as:

$$T = \frac{1}{p} \qquad (7)$$

Thus, the empirical frequencies (or return periods) of AMPs can be estimated for different rainfall durations, and inversely, the AMP quantiles for a given duration can be computed for specific return periods. The empirical IDF curves can hence be plotted as shown in Figure 8.
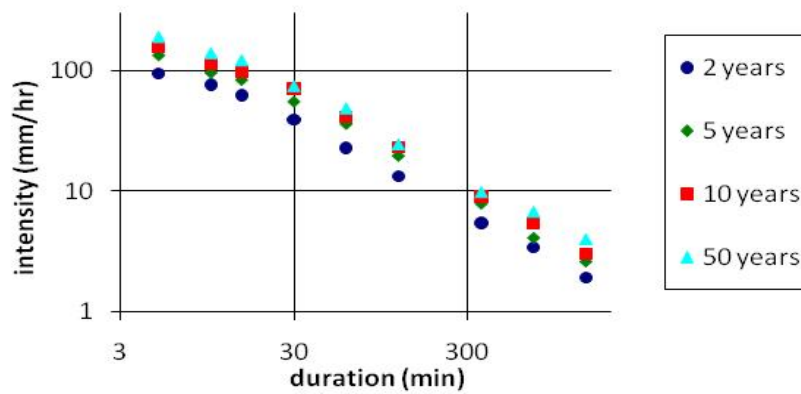
Figure 8: Empirical IDF curves for the 1961-1994 baseline period

3.2.1.4. Temporal downscaling

There are empirical evidences that some characteristics of short-duration rainfalls can be deduced from longer duration extreme events (Over and Gupta, 1994, Aronica and Freni, 2005; and Nhat et al., 2006). Indeed, extreme precipitation events often present scale invariance properties (Burlando and Rosso, 1996). This scaling concept can be expressed as:

- If a function f is scaling invariant, there is a constant β such that:

$$\forall x, \quad f(\lambda x) = \lambda^\beta f(x) \tag{8}$$

Nguyen et al. (2002) proved that such functions can be formulated as:

$$\forall x, \quad f(x) = x^\beta f(1) \tag{9}$$

Hence, the NCM, for a duration t, can be presented in a similar formulation:

$$\forall k \in \mathbb{N}^*, \ \mu_k(t) = E\{f^k(t)\} \tag{10}$$

$$\mu_k(t) = E\{f^k(1)t^{\beta k}\} \tag{11}$$

$$\mu_k(t) = E\{f^k(1)\}t^{\beta k} \tag{12}$$

As a consequence, the three GEV parameters and the quantile $X\tau$ for sub-daily durations can be computed from daily GEV parameters using these properties (Nguyen et al., 2006):

$$\kappa(\lambda t) = \kappa(t) \tag{13}$$

$$\alpha(\lambda t) = \alpha(t)\lambda^\beta \tag{14}$$

$$\xi(\lambda t) = \xi(t)\lambda^\beta \tag{15}$$

$$X_\tau(\lambda t) = X_\tau(t)\lambda^\beta \tag{16}$$

It should be noticed that precipitations can present different scaling regimes. In other words, they can exhibit scale invariance properties, with different scaling parameters (i.e. different β) during distinct duration intervals (called scale

interval). For example, if a function has two scaling regimes, one between t_1 and t_2, and the other one between t_2 and t_3, the function can be described as:

$$\begin{cases} \forall t \in [t_1; t_2] & f(t) = \left(\frac{t}{t_2}\right)^{\beta_1} f(t_2) \\ \forall t \in [t_2; t_3] & f(t) = \left(\frac{t}{t_3}\right)^{\beta_2} f(t_3) \end{cases} \qquad (17)$$

Thus, the IDF curves can be fully defined with only the three estimated parameters for the GEV distribution for the daily duration and the scaling parameters corresponding to the different extreme rainfall scaling regimes.

3.2.2. Estimation of Runoff Volumes and Peak Flows

3.2.2.1. Watershed Configurations

Different typical urban watersheds have been considered in this part. Their characteristics are listed in Table 2. They represent some of the configurations (imperviousness, area, shape) representative of cities in Quebec.

TYPE	PERCENT OF IMPERVIOUSNESS(%)	AREA (ha)	Shape
Parking lots	100 %	0.4 and 2	rectangular
High density residential area	65 %	1 and 10	square

Table 2: Watershed configurations

For illustration purposes, only the results of the small residential area configuration (square, 65%, 1 ha) are presented in the text and the results for the other watershed configurations are described in Appendice E

3.2.2.2. Storm Water Management Model (SWMM)

The Storm Water Management Model (SWMM) developed by the US Environmental Protection Agency is widely used for the estimation of urban runoff from rainfall (Huber and Dickinson, 1988). Discrete rainfall hyetographs are used as input for this model. As the purpose of this study is not to investigate the performance of the SWMM but to assess the ability of the proposed downscaling method to mimic actual precipitation pattern and to estimate the evolution of runoff characteristics due to change in precipitation patterns; hence, no specific calibration of the SWMM is necessary. Indeed, comparisons between runoff properties computed from synthetic design storms were compared with those given by the observed real storms to assess the accuracy of the suggested estimation method.

In the first step, the runoff values generated by the 136 historical storms were first computed. Annual maximum volumes and peak flows were extracted from the results and a frequency analysis of these two extreme series was carried out. The Gumbel distribution (Extreme Value Type I) provides the best fit for these runoff value (Mailhot et al., 2007b). Thus the empirical quantiles for the runoff values can be expressed as:

$$X_T = \bar{X} + K_T S_X \qquad (18)$$

$$K_T = -\frac{\sqrt{6}}{\pi}\{0.5772 + ln(ln(T) - ln(T-1))\} \qquad (19)$$

where $\bar{X}$ is the mean of the runoff volume (or peak flow) and S_X the standard deviation.

In the second step, synthetic hyetographs for current and future periods were used to validate the computed runoff for the current period and to make the projection of runoff for future periods. These synthetic hyetographs are called (synthetic) "design storms".

3.2.2.3.　Design Storms

3.2.2.3.1.　General consideration

Peyron (2001) has demonstrated that three design storm models proposed by Desbordes (1978), Watt et al. (1986), and Peyron et al. (2001) could provide runoff properties that are similar to those given by the observed historical storms. These three design storm models were thus chosen for this study. More specifically, the selected design storms were computed for different return periods based on the computed IDF curves for Dorval Airport as described previously. In addition, all these synthetic storms have 1-hour duration with a discrete time step of 5 minutes.

3.2.2.3.2.　Desbordes Design Storm

Figure 9 shows the shape of the Desbordes design storm. The maximum intensity is located at the 25th minute of the 1-hour storm duration.

Notation:

$I_d = maximal\ intensity\ for\ duration\ d, for\ a\ given\ return\ period$

$J = average\ intensity\ in\ the\ complementary\ intervals,$

$\qquad (before\ 10\ min\ and\ after\ 40\ minutes)$

$$J = \frac{60\,I_{60} - 30\,I_{30}}{60 - 30} = 2\,I_{60} - I_{30}$$

Equation

$$i(t) = \begin{cases} \dfrac{2*J*t}{10} & for\ t \in [0;10] \\[2mm] 2*J + 2\dfrac{(I_{30}-J)}{30/2}*(t-10) & for\ t \in\ ]10;25] \\[2mm] 2*J + 2\dfrac{(I_{30}-J)}{30/2}*(10+30-t) & for\ t \in\ ]25;40] \\[2mm] 2*J - 2\dfrac{J}{(60-10-30)}*(t-10-30) & for\ t \in\ ]40;60] \end{cases}$$

18
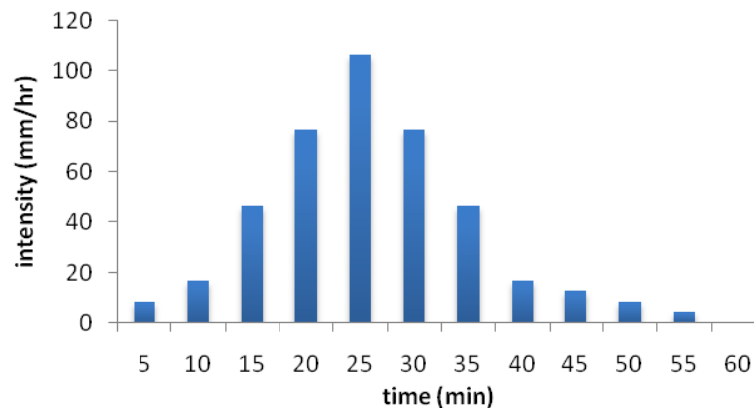
Figure 9: Example of a Desbordes Design Storm
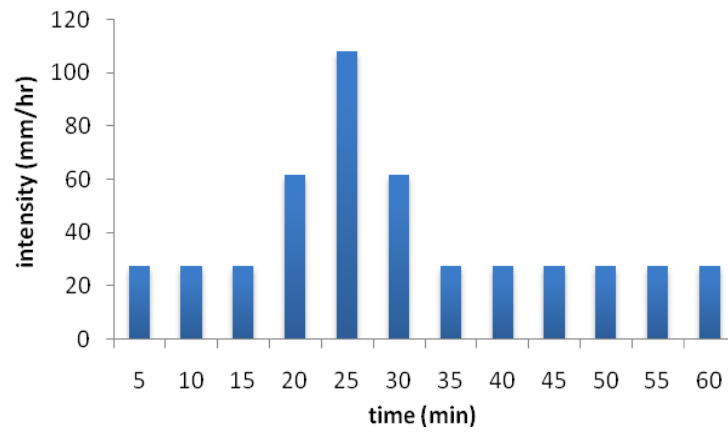
Figure 10: Example of a Peyron Design Storm
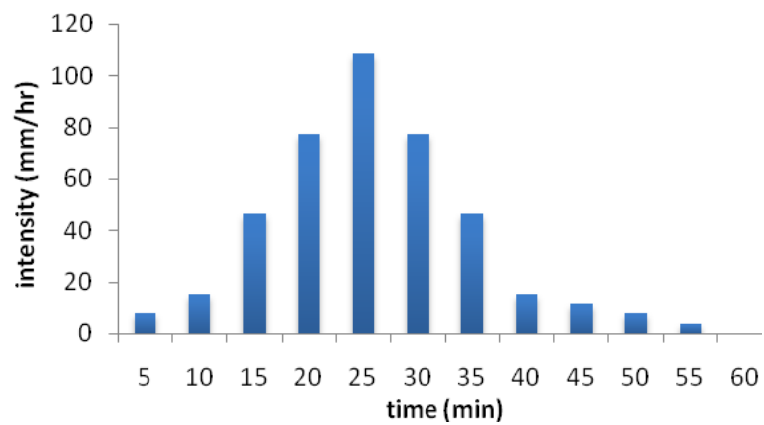
Figure 11: Example of a Watt et al. Design Storm

3.2.2.3.3. Peyron Design Storm

The period of maximal intensity lasts 15 minutes between the 20th and 35th minutes and the intensity peak occurs at the 25th minute (Figure 10). The intensity is constant outside of the interval. This design storm generates a total depth 1.3 times higher than the actual 1-hour maximal volume for the same return period.

Equation:

$$i(t) = \begin{cases} \dfrac{(1.3 * I_{60} * 60 - 5 * (1.4 + 2 * 0.8)I_{15})}{5 * 9}, & for\ t \in [0; 20[\ \cup\ ]35; 60] \\ 0.8 * I_{15} & , for\ t \in [20; 25[\ \cup\ [30; 35[\\ 0.8 * I_{15} & , for\ t \in\ [25; 30[\end{cases}$$

3.2.2.3.4. Watt Design Storm

The maximum of intensity takes place in the 5th time interval (Figure 11).

Equation:

$$i(t) = \begin{cases} I_5 * \dfrac{t}{27} & , \quad for\ t \in [0; 25] \\ I_5 * exp(-7(t - 27)/(60 - 27)), & for\ t \in\ ]25; 60] \end{cases}$$

3.3. Results and Discussion

3.3.1. Verification and Validation Process

In order to assess the feasibility of the proposed downscaling procedure to generate accurate runoff properties for the current and future periods. The accuracy of the scaling GEV distribution in the estimation of AMPs for different durations is evaluated.

3.3.1.1. Accuracy of the Scaling GEV

In order to assert the ability of the GEV distribution to fit observed data, quantile plots were drawn for each of the 9 durations (Figure 12 and APPENDICES D). The goodness-of-fit found for all the durations corroborates the hypothesis of AMPs following GEV distributions.

20
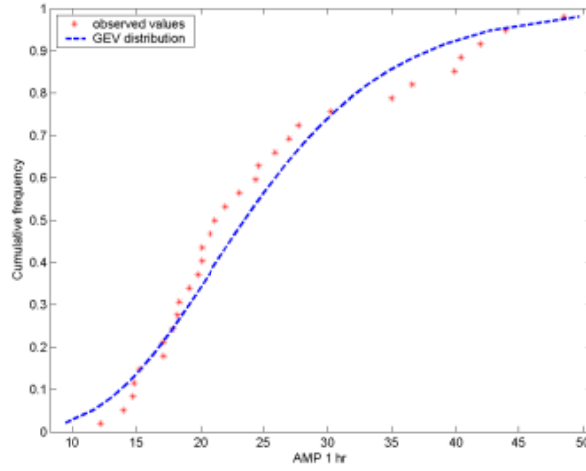
Figure 12: Quantile plots of the 1hr AMP for the baseline 1961-1994 period

The scaling behaviour of the AMP recorded at the station is investigated by plotting the logarithm of the NCM from the AMP series, against the logarithm of the duration. Indeed, as previously demonstrated, the non central moments of a scaling function could be written as

$$\mu_k(t)=E\{f^k(1)\}t^{\beta k} \tag{20}$$

So $$ln(\mu_k(t))=ln(E\{f^k(1)\})+\beta k\,ln(t) \tag{21}$$

Thus, if the function is scaling, the plot should be linear and the slopes would be proportional with a factor β.
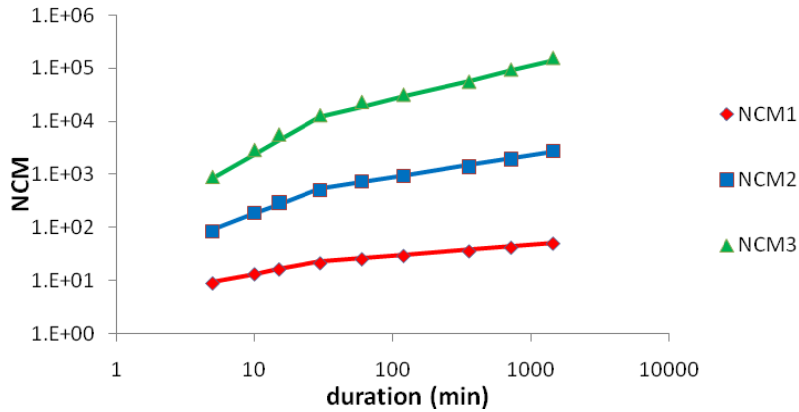
Figure 13: Linearity of the NCM of AMPs for the baseline 1961-1994 period

Hence, the linearity of the graphs exhibited on Figure 13 and on Figure 14 indicates the scaling behaviour of the AMPs at Dorval airport. In particular, there are two different scaling regimes: the first one between 5 and 30 minutes (β_1=0.50) and the second between 30 minutes and 1 day (β_2=0.21).
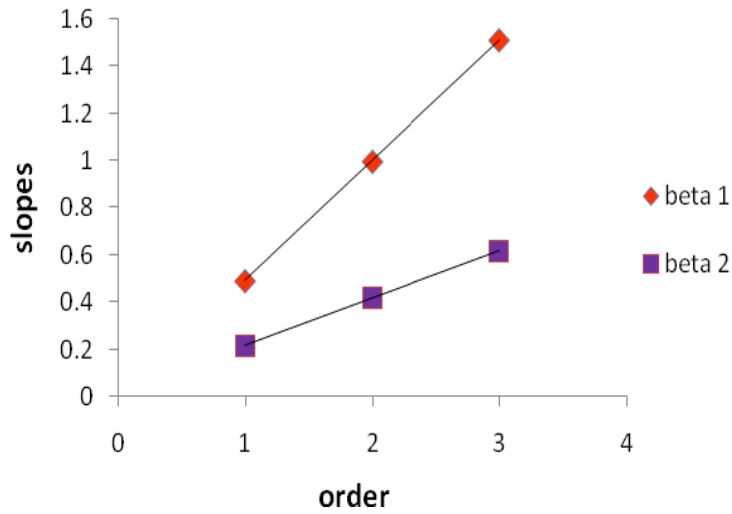
Figure 14: Linearity of the scaling slopes (β*k)

Based on the two estimated scaling parameters β_1 and β_2, the three NCMs and the corresponding GEV distribution parameters for the 8 sub-daily durations were derived from the three NCMs and the associated computed GEV parameters for the daily AMP. On the basis of these GEV distributions, the AMP quantiles were computed, and the resulting IDF curves were derived. As indicated by Figure 15, the estimated IDF curves (lines) agreed very well with the empirical ones (symbols) (R^2~0.99). Hence, the proposed NCM/scaling GEV method can provide accurate description of the AMP distributions.
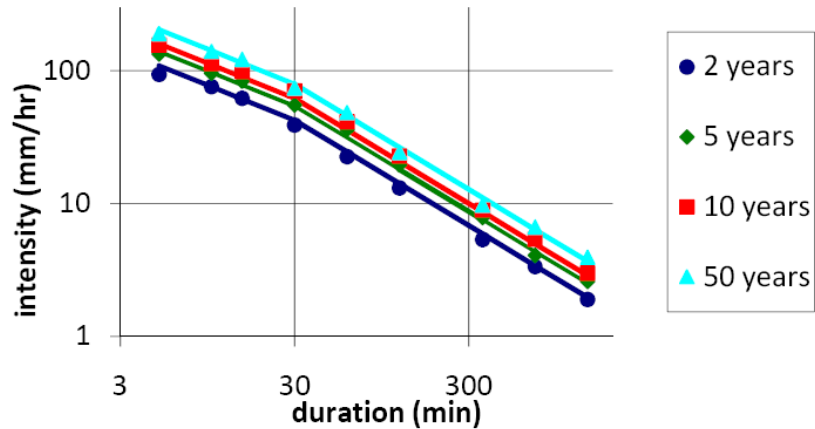
Figure 15: IDF Curves built with scaling concept for the baseline period
symbols= observed values and line = Scaling GEV model

3.3.1.2. Estimation of runoff properties

The three different design storms (Figure 16) were derived using the computed IDF curves as described above. These design storms were then used as input to the SWMM model to estimate the corresponding runoff peaks and volumes for the selected urban watersheds. Similarly, these two runoff properties were computed for the historical storms using the SWMM simulation with the same conditions as for the synthetic design storms.

As expected, the Watt design storm model gave the best performance in the estimation of the runoff volumes, while the (Figure 17 and Tables 3 and 4) Desbordes model provided an accurate estimation of the peak flows (Figure 18 and Table 4), and the Peyron model gave accurate estimations for both of these runoff properties.
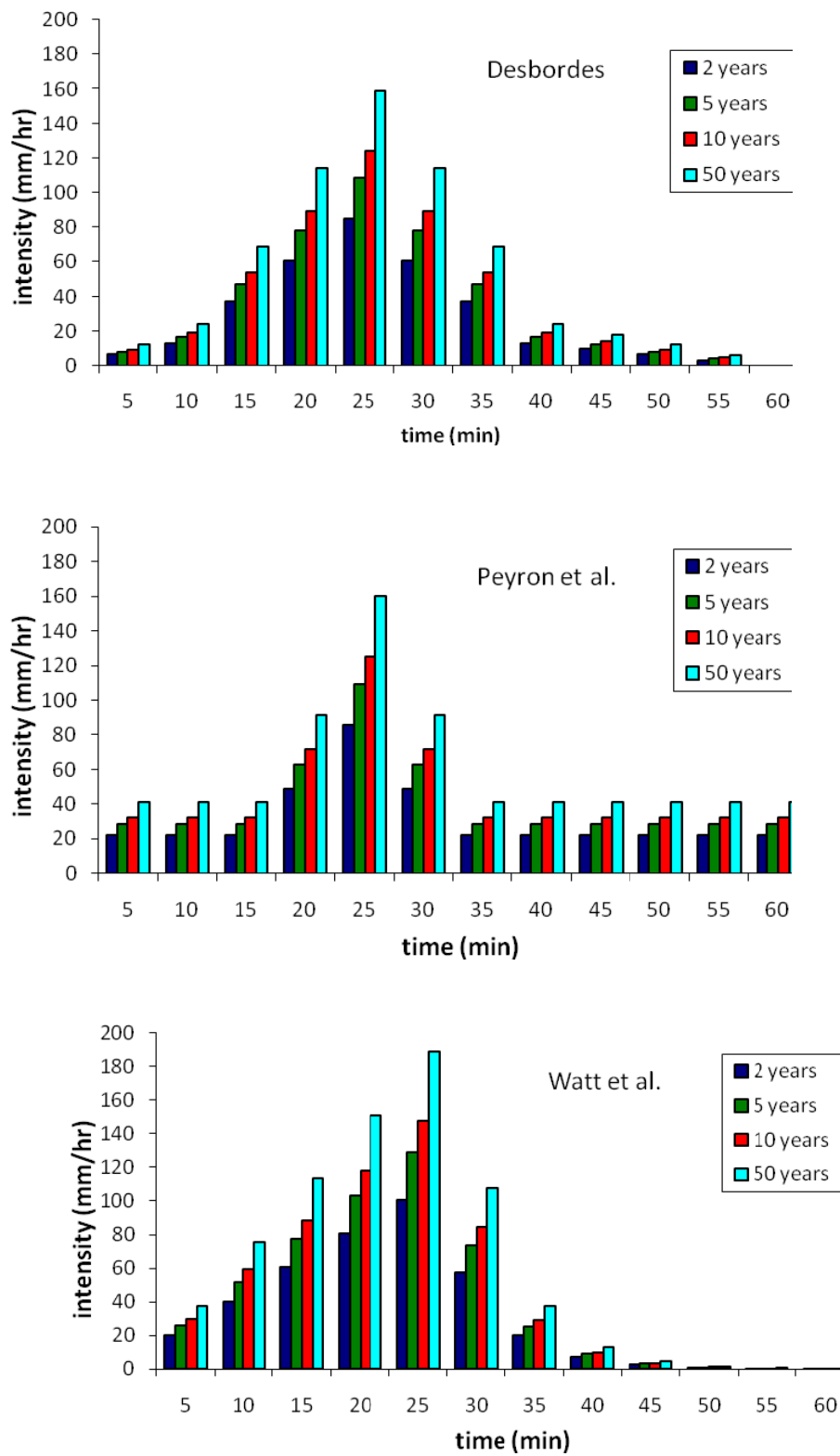
Figure 16: Three design storms from the observed data for the 1961-1994 baseline period
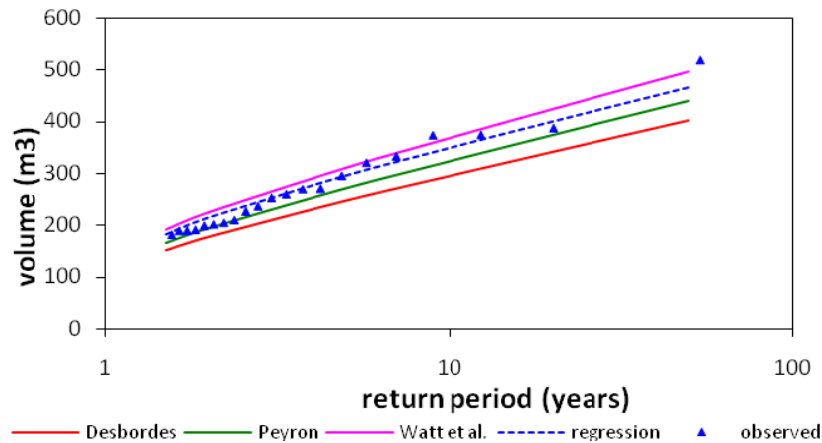
Figure 17: Estimation of runoff volumes from three design storms and from observed storms for the 1961-1994 baseline period

Volume	2 years	5 years	10 years	50 years
Desbordes	-17,35%	-16,21%	-15,29%	-13,40%
Peyron	-9,57%	-8,19%	-7,14%	-5,23%
Watt et al.	4,21%	4,93%	5,59%	6,95%

Table 3: Difference between volumes generated from the observed storms and from the design storms
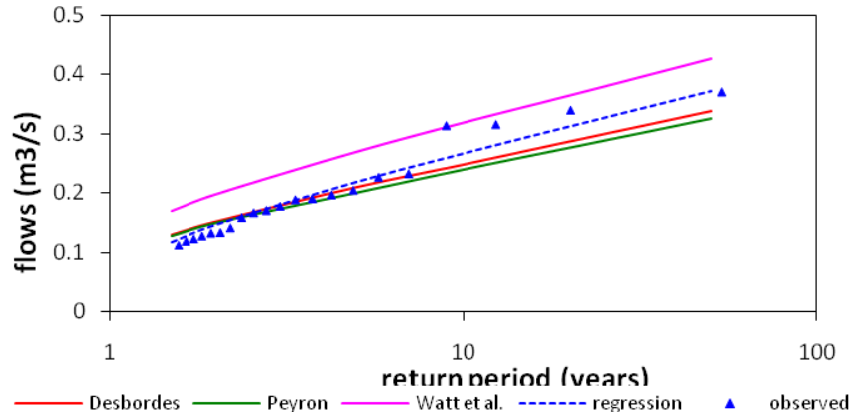
Figure 18: Estimation of peak flows from the three design storms and from observed storms for the 1961-1994 baseline period

peak flow	2 years	5 years	10 years	50 years
Desbordes	4,51%	-3,56%	-6,64%	-8,90%
Peyron	2,46%	-8,14%	-10,01%	-12,39%
Watt et al.	35,25%	23,40%	19,61%	14,75%

Table 4: Difference between peak flows generated from the observed storms and from the design storms

25

3.4. Validation

The downscaled daily rainfall series were generated using the calibrated SDSM procedure for two GCMs (the UK HadCM3 and the Canadian CGCM2) for the 1961-1979 period. The design storms and the resulting runoff peak flows and volumes were then estimated based on the 100 generated downscaled daily rainfall time series and the bias-correction procedure as suggested in section 2.1.4. for the 1980-1994 period (Figure 19 and 20). The computed runoff values from design storms were compared with those from historical storms for the 1980-1994 period.
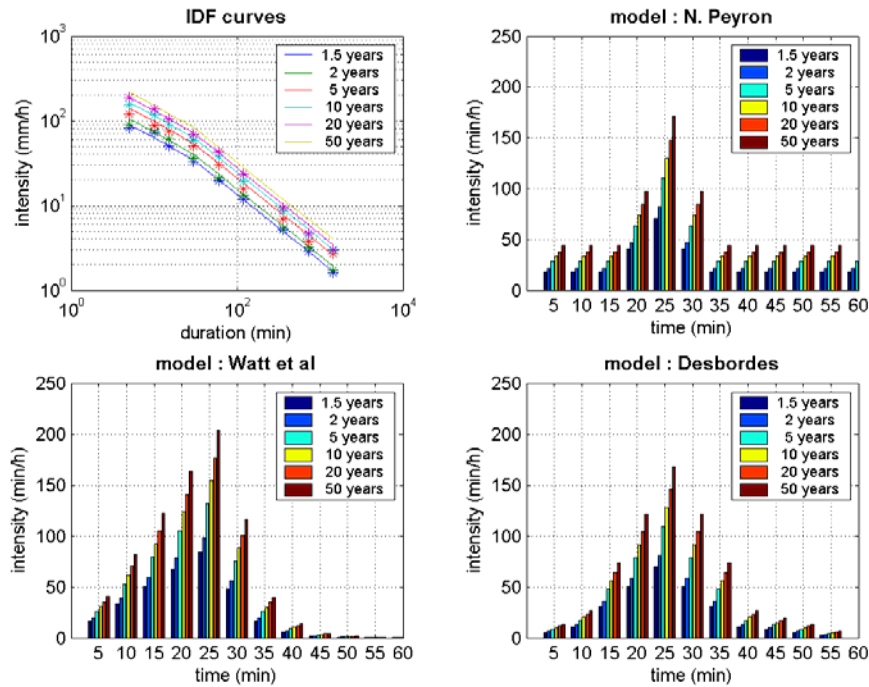
Figure 19: IDF and design storms estimated based on SDSM downscaling results using CGCM2 predictors for 1980-1994, with parameters calibrated over the 1961-1979 period

Comparable results were found for runoff values computed for these two cases for both HadCM3 and CGCM2 models (Tables 5 and 6, Figures 21 and 22). The differences range from 0.5 to 10% for the runoff volumes using Watt model and between 0.6 and 11.5 % for the peak flows using Desbordes model. Hence, the

proposed procedure is able to produce consistent IDF curves and to provide good estimations of runoff values when an appropriate design storm model was selected.
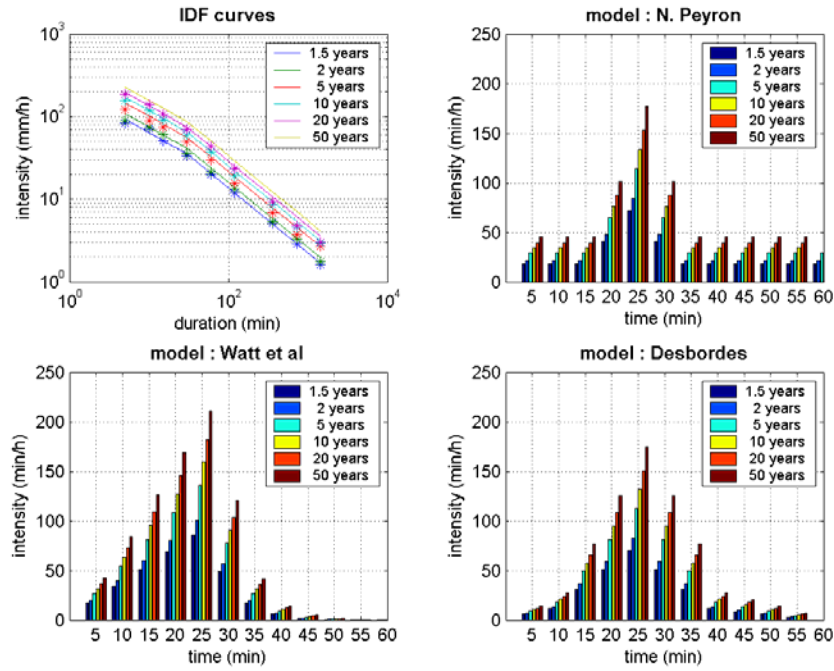
Figure 20: IDF and design storms conceived from SDSM driven by HadCM3 for 1980-1994, with parameters calibrated over the 1961-1979 period
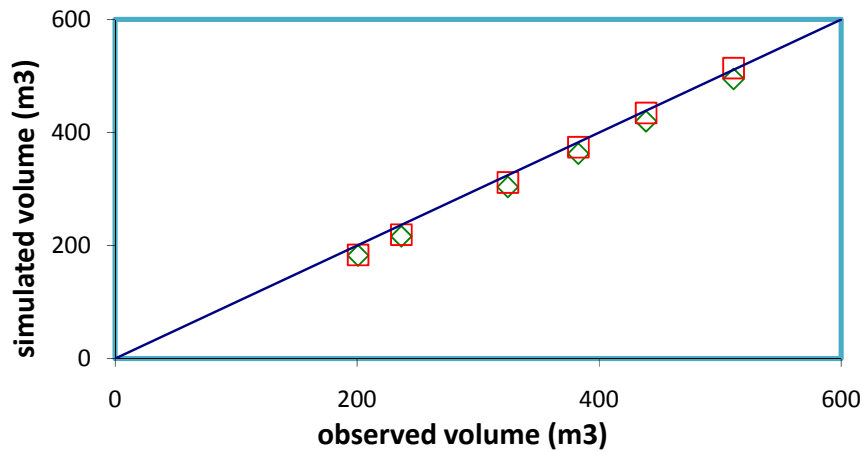
Figure 21: Simulated runoff volumes from the GCMs using Watt design storm model as compared with the volume from the historical storms (diamond= CGCM2 and square HadCM3)

VOLUMES	Return period (years)					
Desbordes	1,5	2	5	10	20	50
CGCM2	-28,1%	-28,1%	-26,1%	-24,8%	-23,6%	-22,3%
HadCM3	-27,8%	-27,2%	-24,1%	-22,3%	-20,8%	-19,2%
Peyron	1,5	2	5	10	20	50
CGCM2	-21,9%	-21,7%	-19,4%	-17,9%	-16,7%	-15,4%
HadCM3	-21,5%	-20,7%	-17,2%	-15,2%	-13,6%	-12,0%
Watt et al.	1,5	2	5	10	20	50
CGCM2	-9,1%	-8,5%	-6,5%	-5,3%	-4,3%	-3,2%
HadCM3	-8,6%	-7,3%	-4,0%	-2,3%	-0,9%	0,5%

Table 5: Difference (in %) between volumes generated from the observed storms and from different design storm models for different return periods
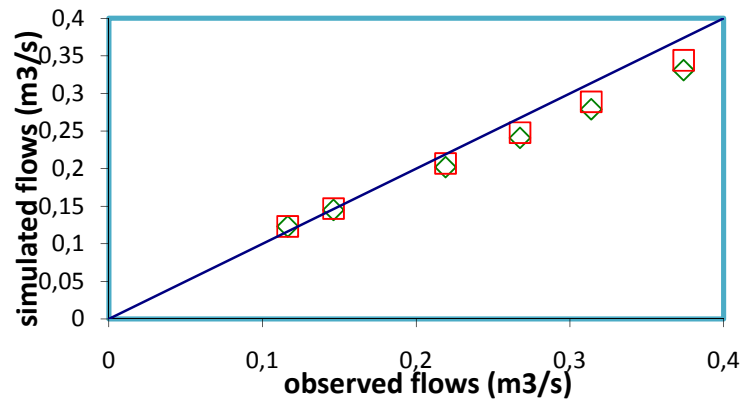
Figure 22: Simulated peak flows from the GCMs using Desbordes design storm models as compared with peakflows from the observed storms(diamond= CGCM2 and square HadCM3)

FLOWS	return period (years)					
Desbordes	1,5	2	5	10	20	50
CGCM2	5,7%	-0,8%	-7,8%	-9,9%	-11,1%	-11,5%
HadCM3	5,7%	0,6%	-5,5%	-7,3%	-7,9%	-8,0%
Peyron	1,5	2	5	10	20	50
CGCM2	4,0%	-2,8%	-11,0%	-12,9%	-14,0%	-14,4%
HadCM3	4,0%	-1,4%	-9,2%	-10,3%	-10,8%	-10,9%
Watt et al.	1,5	2	5	10	20	50
CGCM2	39,2%	30,7%	20,5%	17,4%	15,0%	13,7%
HadCM3	39,2%	32,1%	23,7%	20,7%	19,1%	17,9%

Table 6: Difference (in %) between peak flows generated from the observed storms and from different design storm models for different return periods.

3.4.1. Simulations for future periods

3.4.1.1. IDF Curves for future periods

As part of the reliability of the results depends on the length of the calibration period, the calibration steps take into account all the observed data (i.e. the calibration period will be the baseline periods, 1961-1994, without the 3 years with inconsistent data). IDF curves, design storms and runoff estimations are produced for the baseline period using SDSM-GCM unbiased daily simulations and the three future periods (2020s, 2050s and 2080s), for both GCM (CGCM2 and HadCM3).

The GCM provides two different trends for future extreme rainfalls (Figures 24 and 26). Even if both predict a small decrease of intensities, for all return periods, during the first period (2020s), the downscaled runs using the CGCM2 predictors show a significant increase (~ +10%) for the last 2 periods (2050s, 2080s), whereas the HadCM3 indicates a continuously slight decrease (reaching ~ -4% in 2080s). However, these changes are not identical in proportions for the different return periods. Indeed, according to the results obtained from CGCM2 outputs (Figures 23 and 24), the decrease during the first 30-year period is more pronounced for the rarest events (i.e. with the biggest return periods), but the relative increase in one century would be approximately the same for all the return period. The data from HadCM3 model provides different results (Figures 25 and 26). The small decrease in intensity will be fairly similar between the different frequencies of events.
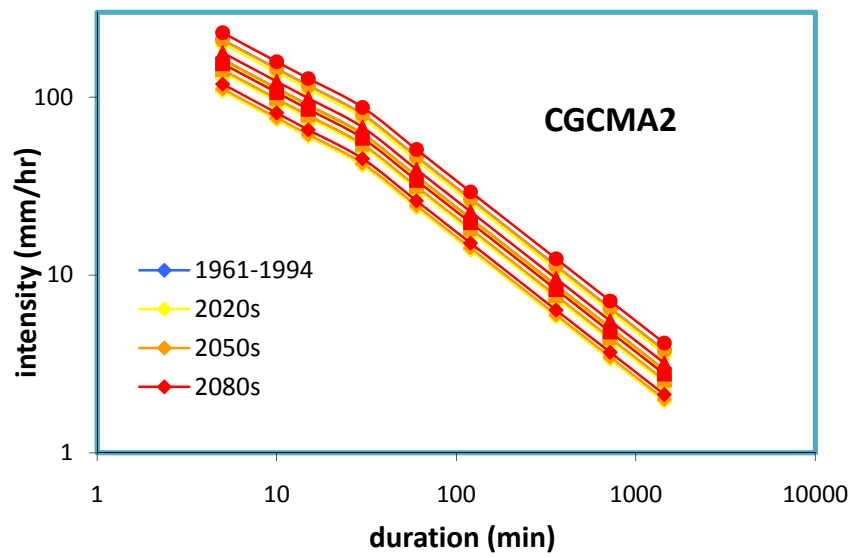
Figure 23: IDF Curves generated from SDSM-CGCM2unbiased daily precipitation, for current and future periods
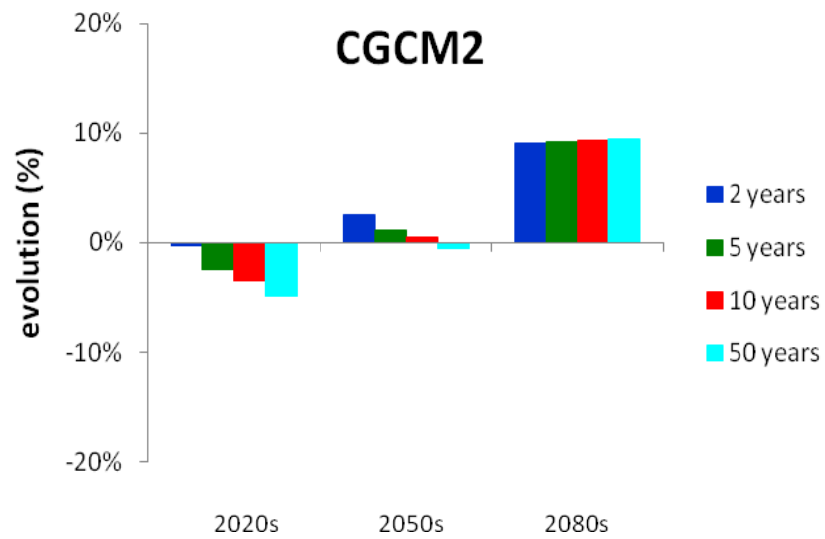
Figure 24: Evolution of the daily intensity according to SDSM-CGCM2 with respect to the the baseline period
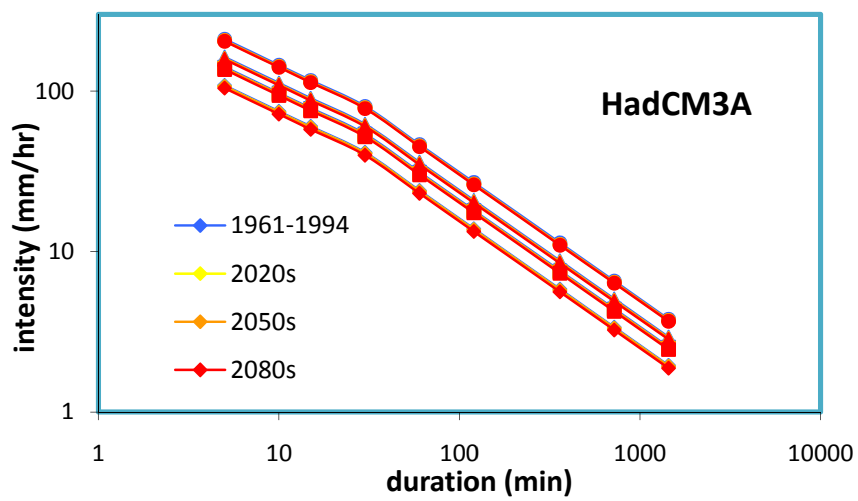
Figure 25: IDF Curves generated from HadCM3, for current and future periods
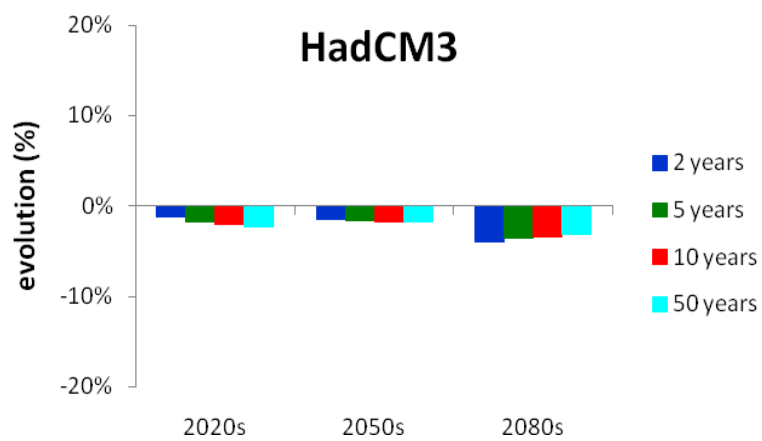
Figure 26: Evolution of the daily intensity according to HadCM3 in comparison with the baseline period

3.4.1.2. Design Storms

CGCM2

HadCM3
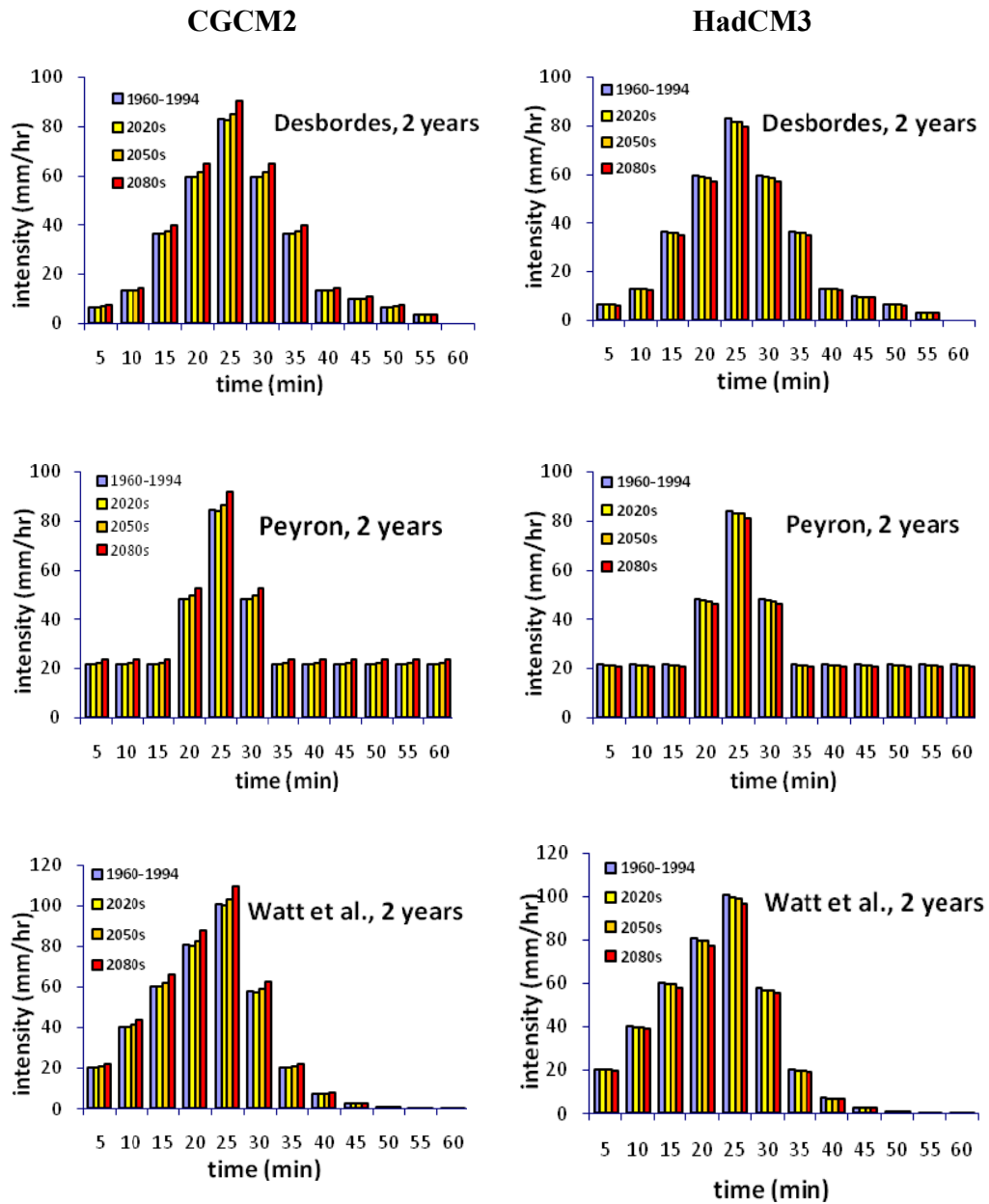
Figure 27: Design storms for the current and future periods, with a 2-year return period, from both SDSM-GCM.

The design storms are built based on these new curves (e.g. for the 2-year return period, Figure 27 or Appendices E, Figures 40-43). As expected, the change of the rainfall intensities are similar to the ones noticed in the IDF curves, with a slight reduction when the hyetograph are computed based on HadCM3 inputs and an increase when CGCM2 predictors are used in the downscaling process.

3.5. Future Runoff estimations

SWMM simulations were performed for the different watershed configurations. Again, the results exhibit different trends according to the GCM selected (Figures 28 and 29). Again, the same conclusions can be drawn: Two different changes are probable, increase according to CGCM2 (despite the initial decrease) and slight decrease with HadCM3.
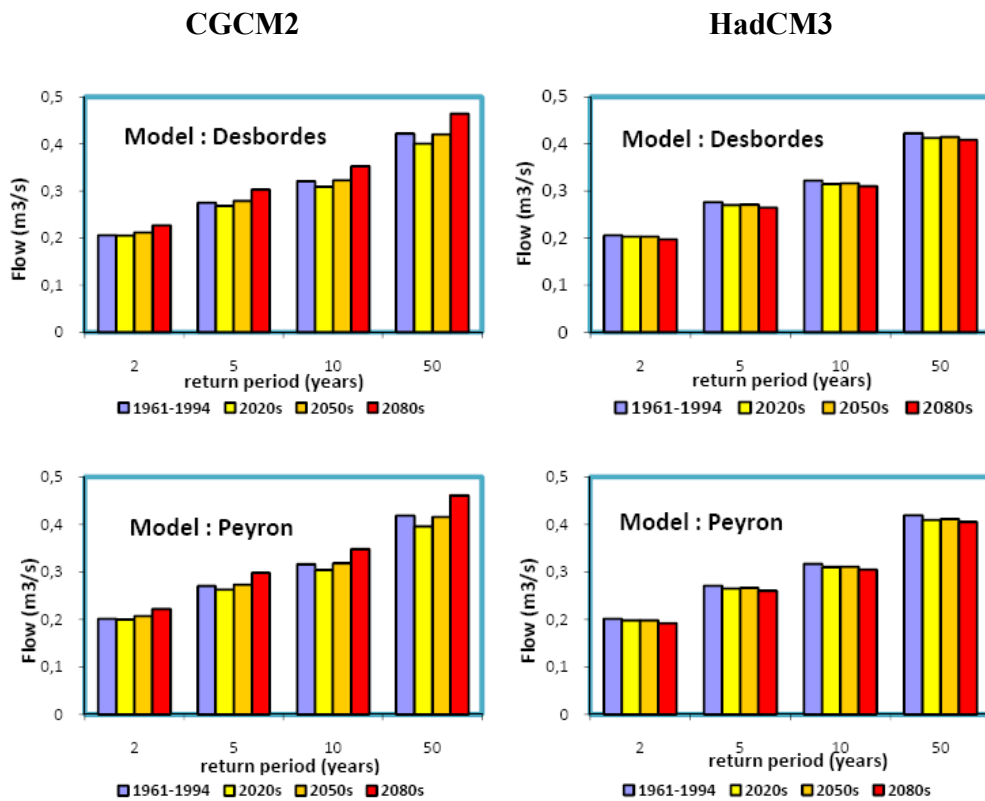
CGCM2   **HadCM3**

Figure 28: Evolution of the runoff peak flows (Watershed: square, 65%, 1ha)

CGCM2
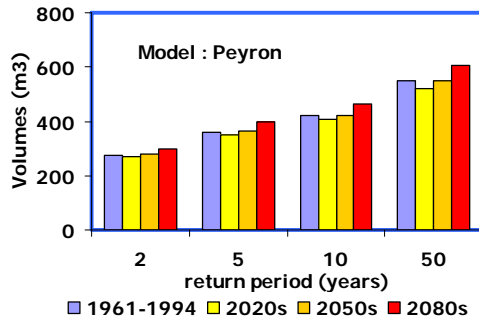
HadCM3
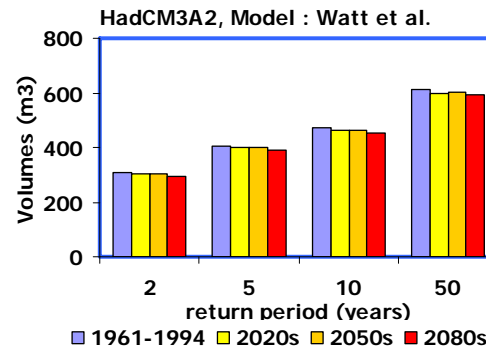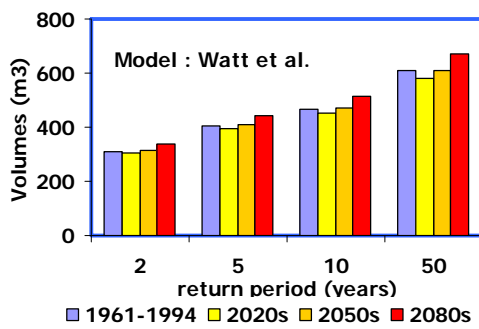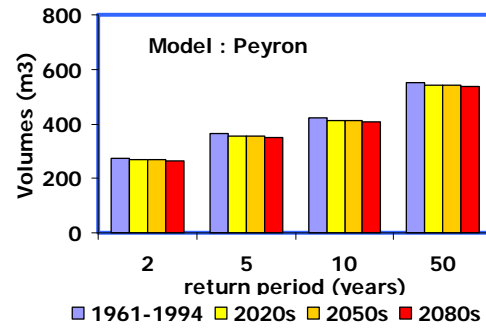
Figure 29: Evolution of the runoff volume, (Watershed: square, 65%, 1ha)

3.6. Discussion

As the different results illustrate, there are contradictories information provided by the two different GCM, with opposite consequences. According to the simulations based on the UK HadCM3, runoff values will decrease, so the drainage systems would not require to be retrofitted. But, the runoff values generated from the Canadian CGCM2 tend to predict a potential future overwhelming of the drainage network. So uncertainties remain on the capacity of the drainage system to carry out runoff water. These uncertainties seem due to the inherent uncertainties in the downscaling results using different GCMs (i.e. the main sources of uncertainties are in the scenarios) Hence the proposed procedure appears to provide reliable estimations for current climate, but no clear signal can be exploited for future periods due to the inherent uncertainties of the GCMs.

3.7. Future studies

Even if the procedure proposed in the present study seems to be reliable, further studies are necessary to address the following issues:

- Other GCMs and greenhouse gases emission scenarios should be investigated to provide a wider range of probable runoff evolutions.

- The potential impacts of climate change on the scaling behaviour of extreme rainfall processes need to be investigated to avoid the assumption of stationarity in the rainfall scaling parameters for current and future periods (one possible approach is to find the linkage between the scaling parameters and the climatic conditions).

4. Regional analysis of rainfall scaling properties

4.1. Introduction

As indicated in Chapter 2, one of the main advantages of the scaling GEV approach is its ability to determine the extreme precipitation distributions for different durations based only on a few parameters; that is, the three parameters of the GEV distribution for a given duration and the two slopes of the rainfall scaling functions. However, the estimation of these two slopes requires a certain amount of rainfall data that may not be sufficiently available or that may not exist for the site of interest. In order to cope with these issues, this section investigates the regional variability of the rainfall scaling parameters. In addition, as mentioned in Section 2.7, this regional analysis could be useful in dealing with the projections of rainfall scaling parameters for future periods in the context of climate change.

4.2. Regional analysis

4.2.1. Case study using rainfall data in Singapore

The regional analysis is performed using rainfall records available at nine raingages located on the Singapore Island (1.20 N 103.50 E, 585 km², Figure 30). The selection of Singapore location for this case study was based on the more homogeneous climatic conditions over the whole 585-km^2 Singapore area as compared to the high regional climate variability over the large region of Quebec. Two different sets of data were available for each station in Singapore: the AMP for 8 durations (15, 30 and 45 minutes; 1, 3, 6, 12 and 24 hours) and the daily rainfalls (a day is considered as a rainy day in this study if there is any trace of rainfall recorded). All the data were given in millimetres, with a precision of 0.1 mm for the daily rainfall and 1mm for the AMP. The periods of data availability differ between each station (Table 7), so the study is performed on the first 30-year common period, 1972-2001.

Stations	Daily Rainfalls	Annual Maximum Precipitations
Ama Keng	1961-2007	1960-2007 (1978)[2]
Changi	1967-2007	1972-2007
Jurong Industrial	1964-2007	1963-2007
Macritche	1961-2007	1960-2007
Paya Lebar	1961-2007	1960-2007
Seletar	1967-2007	1971-2007
Singapore Orchids	1966-2007	1966-2007 (1969, 70, 76)
St James	1961-2007	1960-2007
Tengah	1961-2007	1971-2007

Table 7: Periods of data availability for daily rainfalls and for AMPs for eight durations

4.2.2. Data Analysis

4.2.2.1. Monthly repartition of the extreme rainfall occurrences

As expected, the days with the annual maximum daily rainfall depths occur mostly during the monsoon periods[3] (either from November to early February for the North-East monsoon, or from July to September for the South-East monsoon). Indeed, as Singapore is located close to the Equator, the Intertropical Convergence Zone (ITCZ) structure covers the area during the winter month and favour regular rainfall events (Chia and Foong, 1991). Table 8 shows the regional variation of the monthly occurrences of AMPs over the whole study region.

---

[2] (years) = data missing for these years

[3] Singaporean National Environment Agency, http://app.nea.gov.sg/cms/htdocs/article.asp?pid=1088
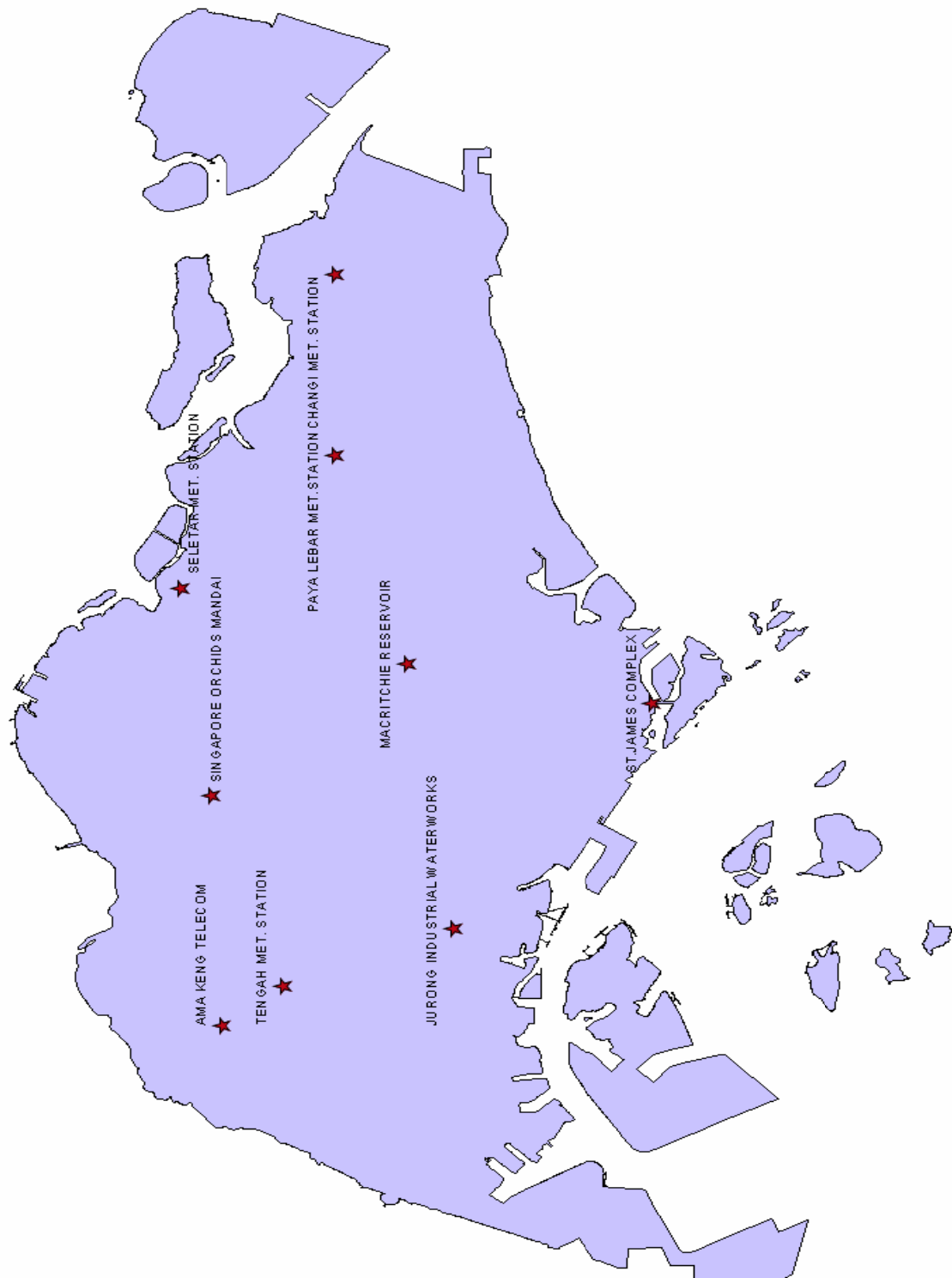
Figure 30: Location of the nine raingage stations in Singapore

Year	Ama Keng	Changi	Juron Ind	Macritche	Paya Lebar	Seletar	Singapore Orchids	St James	Tengah
1972	9	9	12	12	12	9	12	12	9
1973	3	2	4	2	2	2	2	3	10
1974	9	2	9	12	4	4	11	9	11
1975	10	9	2	7	6	8	11	9	10
1976	10	12	12	11	7	7	12	10	10
1977	5	11	8	11	2	7	10	11	10
1978	12	12	12	12	12	12	12	12	12
1979	12	10	11	10	10	7	3	10	10
1980	1	1	5	1	1	1	1	8	1
1981	7	12	7	5	12	5	5	7	7
1982	11	12	4	11	8	12	12	4	12
1983	5	8	7	7	9	5	12	8	5
1984	3	2	3	3	2	6	3	3	9
1985	5	12	5	5	7	9	5	9	5
1986	3	12	3	9	12	4	3	9	3
1987	8	1	3	1	1	1	1	1	10
1988	5	9	5	11	11	11	7	5	5
1989	11	11	8	11	11	11	12	11	11
1990	6	5	4	10	12	9	5	5	12
1991	12	12	12	12	12	12	12	8	12
1992	12	11	11	11	11	11	11	11	11
1993	9	3	3	10	10	3	9	8	3
1994	3	11	11	11	12	6	4	3	6
1995	2	1	7	8	2	2	7	7	2
1996	8	2	4	8	3	3	2	9	2
1997	6	8	8	12	12	5	3	1	8
1998	8	12	1	7	12	12	6	1	8
1999	8	12	11	1	11	5	10	5	8
2000	4	1	4	4	3	1	1	11	3

Table 8 : Number of months of occurrence of annual maximum daily rainfalls

4.2.3. The scaling GEV parameters

The same method described in the previous chapter was used to examine the scaling behaviour of the AMP series at each station. As shown in Figures 31 and 32, the AMPs for every station in Singapore indicate a simple scaling behaviour with two distinct scaling regimes from 15 minutes to 45 minutes and from 45 minutes to one day. Table 9 provides the values of the slopes for the two distinct rainfall scaling regimes for all nine stations.
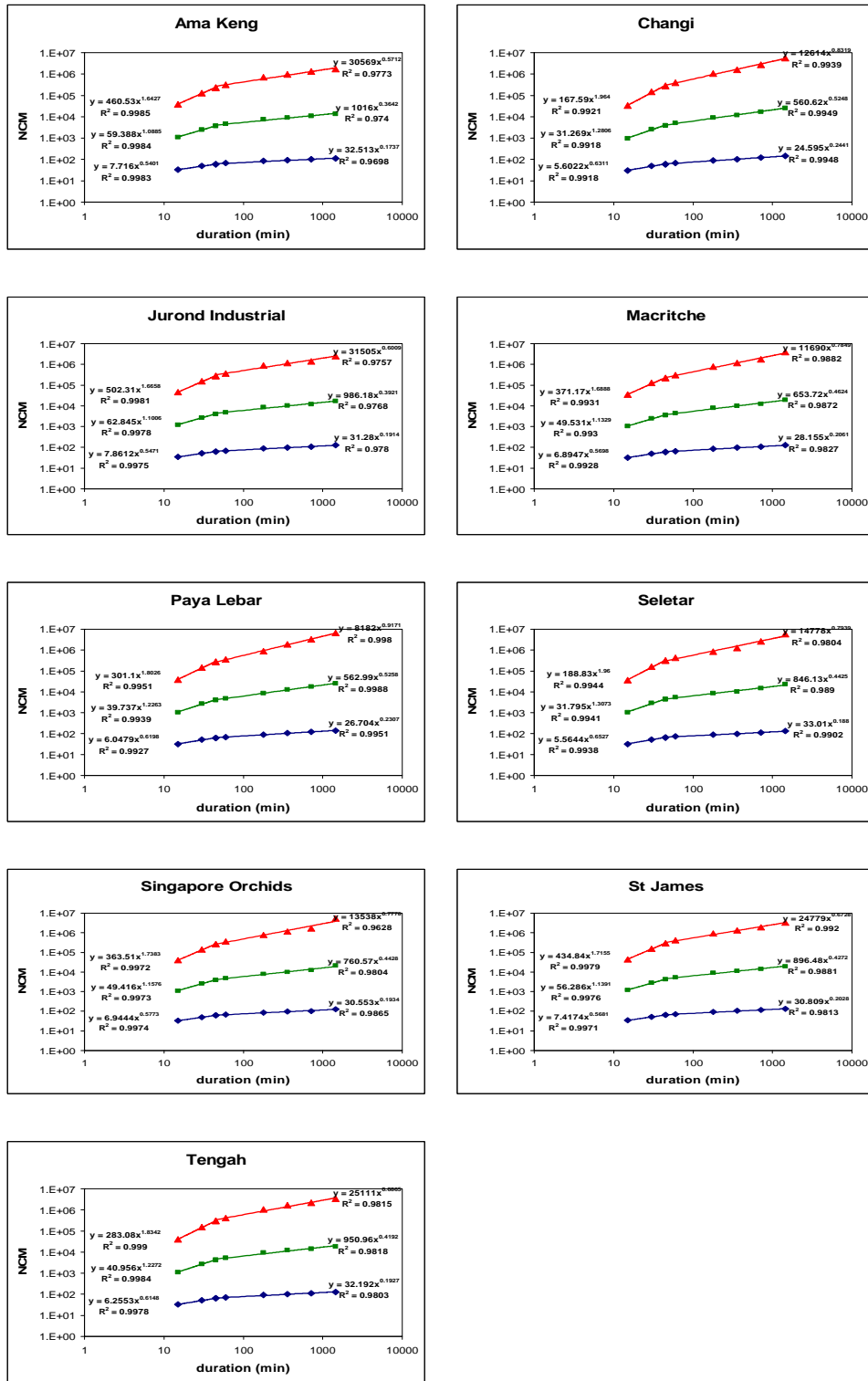
Figure 31: The scaling behaviour of AMPs for nine Singapore stations

40
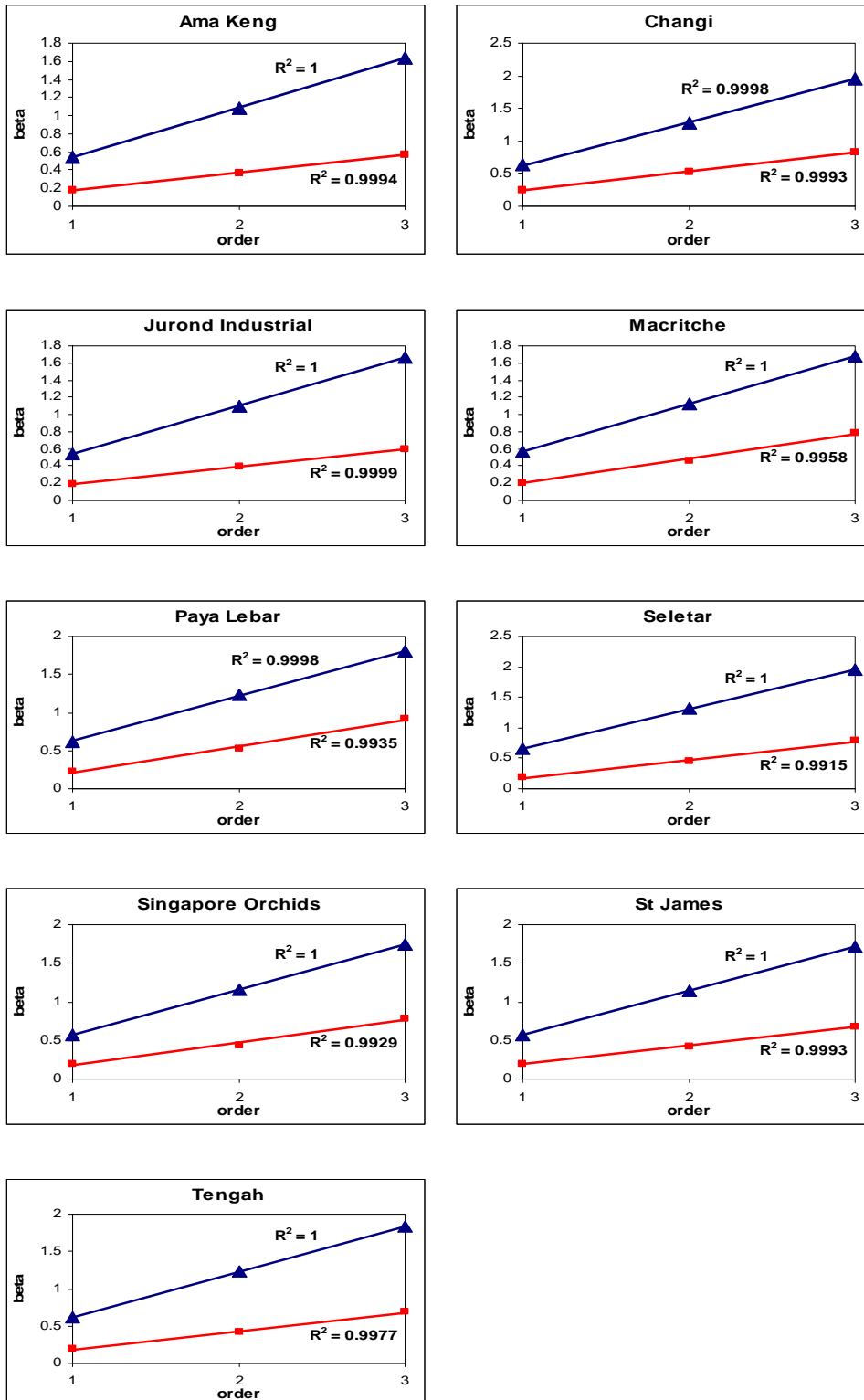
Figure 32: Linearity of the slopes of the rainfall scaling behaviour for nine Singapore raingages

41

	beta 1	beta 2
Ama Keng	0.544	0.182
Changi	0.642	0.261
Jurong Industrial	0.551	0.196
Macritche	0.564	0.233
Paya Lebar	0.611	0.266
Seletar	0.653	0.225
Spore Orchids	0.578	0.225
St James	0.57	0.214
Tengah	0.613	0.21

Table 9: Scaling GEV parameters for nine Singapore stations

4.2.4. IDF Curves

The IDF curves for nine Singapore stations were constructed using the same approach as for Dorval station in Quebec. The three parameters of the GEV distribution for the daily AMP were first estimated, and the GEV parameters for other durations were then computed using the scaling function parameters for the two identified rainfall scaling regimes. Hence, the GEV distributions for all rainfall durations can be estimated using only five parameters (3 daily AMP GEV parameters and 2 scaling slopes). Finally, the IDF curves for each station were estimated from the rainfall quantiles given by these estimated GEV distributions.
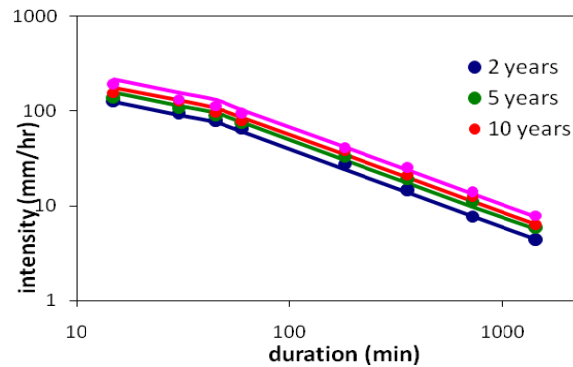
Figure 33: IDF Curves for Ama Keng station derived using Scaling GEV invariance

4.3. Methodology

4.3.1. Assessment of relationships between the scaling function slopes and climatic data

As suggested by Yu et al. (2004), the scaling parameters of AMPs might be related to the number of rainy days at a local site. In order to investigate this linkage, the correlation coefficients between the scaling slopes and the rainfall parameters (either the daily AMPs, the mean number of rainy days per year or per month) were computed. The correlation coefficient is defined as:

$$\sigma_{X,Y} = \frac{E\{XY\} - E\{X\}E\{Y\}}{\sigma_X \sigma_Y} \qquad (22)$$

in which E is the expected value and σ the standard deviation. The relationships are also graphically assessed with plots of the scaling slopes against each of the 14 climatic parameters (average number of rainy days for each month, for the whole year and average AMP for each station for the whole period).

4.3.2. Estimation of GEV parameters for a partially gauged station

In this case, neither the sub-daily AMP nor the scaling slopes but the 14 rainfall parameters are known for the study site. The surrounding stations have all these data. A simple linear regression is established from the surrounding stations, between both scaling slopes and each of the 14 rainfall parameters. Then, using the corresponding parameter at the partially gauged site, the scaling slopes at this site are estimated. The performance of this linear approximation of the scaling slopes is evaluated using the jackknife method; that is, the scaling slopes at each site are supposed missing, then estimated from the other eight surrounding stations, and finally compared with the empirical one at the site, hence, generating 9x2 couples (empirical/estimated) for both scaling slopes.

The performance criterion used is the R² criterion:

$$R^2 = 1 - \frac{\Sigma(\beta_{obs} - \beta_{comp})^2}{(n-1)\ var(\beta_{obs})} \tag{23}$$

In which $\boldsymbol{\beta_{obs}}$ is the empirical value of the scaling slope, $\boldsymbol{\beta_{comp}}$ is the corresponding estimated value, n the number of stations (here, n=9) and $\boldsymbol{var(\beta_{obs})}$ the variance of the series of the empirical values of scaling slopes.

4.3.3. Estimation of GEV parameters for an ungauged station

In this case, it is assumed that rainfall records (i.e., scaling slopes and rainfall parameters) are not available at the site of interest. The procedure is similar to the one used for a partially gauged station, except that the rainfall parameters are estimated from the ones recorded at the other stations using the formula:

$$X_i = \frac{\Sigma_{j=1, j \neq i}^{9} \frac{x_j}{d_{i,j}^2}}{\Sigma_{j=1, j \neq i}^{9} \frac{1}{d_{i,j}^2}} \tag{24}$$

in which $\boldsymbol{X_i}$ is the parameter to be estimated at station i, $\boldsymbol{x_j}$ the corresponding parameter recorded at station j and $\boldsymbol{d_{i,j}}$ the distance between the stations i and j.

4.4. Results

4.4.1. Relationship between scaling slopes and rainfall parameters

The correlation coefficients, computed for every rainfall parameters are shown in Table 10 and some typical results of the linear regressions are displayed on Figures 34, 35 and 36. The scaling slopes are more heavily correlated with the daily AMP and the number of rainy days in January and February. These results could be explained by the fact that these 2 months correspond to the North-East monsoon season, which generates the more intense storms (Chia and Foong, 1991).
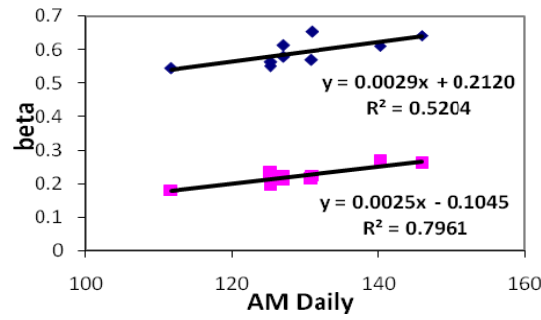
Figure 34: Relation between daily AM and the scaling slopes

So if there are more rainy days in one of these months, it is more likely that there will be an intense storm this year, so shorter duration AMP will increase, and so inversely, the scaling slopes will decrease. In the other hand, if the daily AMPs are high, the scaling slopes are more likely to be high too, to indicate shorter duration AMPs.
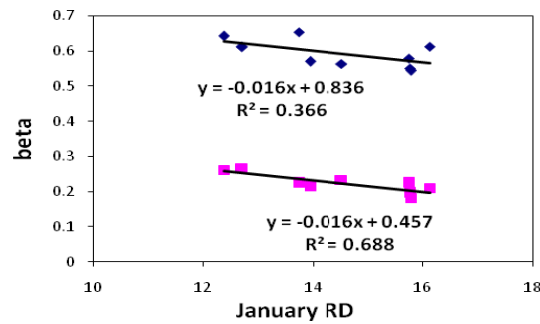
Figure 35: Mean number of rainy days (RD) in January vs. scaling slopes

	beta1	beta2
daily AM	0.72	0.89
annual	-0.08	-0.33
January	-0.61	-0.83
February	-0.51	-0.76
March	-0.38	-0.62
April	-0.18	-0.54
May	0.00	-0.34
June	0.06	-0.19
July	0.25	-0.04
August	0.28	0.12
September	-0.11	-0.01
October	-0.29	-0.61
November	-0.10	-0.24
December	-0.10	-0.26

Table 10: Correlation coefficients between scaling slopes and hydrologic variables.

45
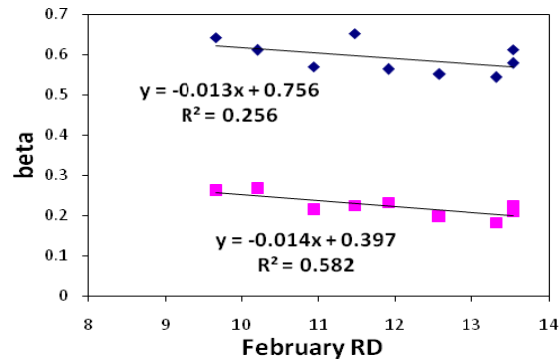
Figure 36: Mean number of rainy days (RD) in February vs. scaling slopes

4.4.2. Estimation of scaling slopes for partially gauged stations

As can be seen from the correlation coefficients, the daily AMP provides the best estimates for both scaling slopes (β_1 and β_2). The number of rainy days in January gives also coherent approximate for the higher duration scaling regime (β_2). The resulting computed scaling parameters obtained with the jackknife method are not too different compared with the observed ones (Table 11, Figures 37 and 38). As a consequence, the scaling slopes can be estimated fairly well with this procedure.

	beta1	beta2
daily AM	0.37	0.70
annual	-0.72	-0.47
January	-0.01	0.48
February	-0.15	0.30
March	-0.47	-0.19
April	-0.55	-0.27
May	-0.67	-0.41
June	-0.55	-0.54
July	-0.45	-0.46
August	-0.66	-0.34
September	-0.42	-0.38
October	-0.51	-0.18
November	-0.72	-0.69
December	-0.56	-0.51

Table 11: Performance criterion (R^2) of the jackknife method for partially gauged stations for the 14 climatic parameters.
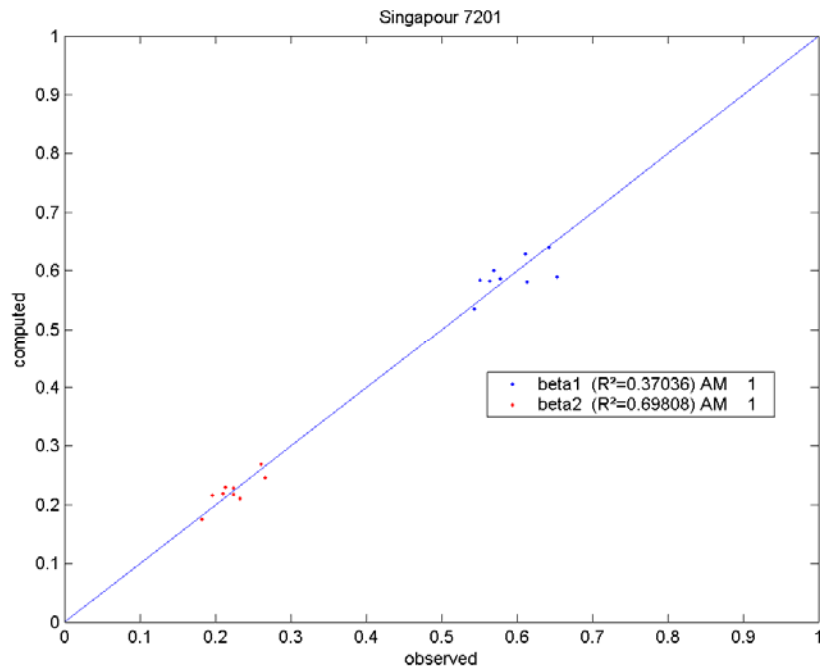
Figure 37: Results of the jackknife method with daily AMP as rainfall parameters for partially gauged site.
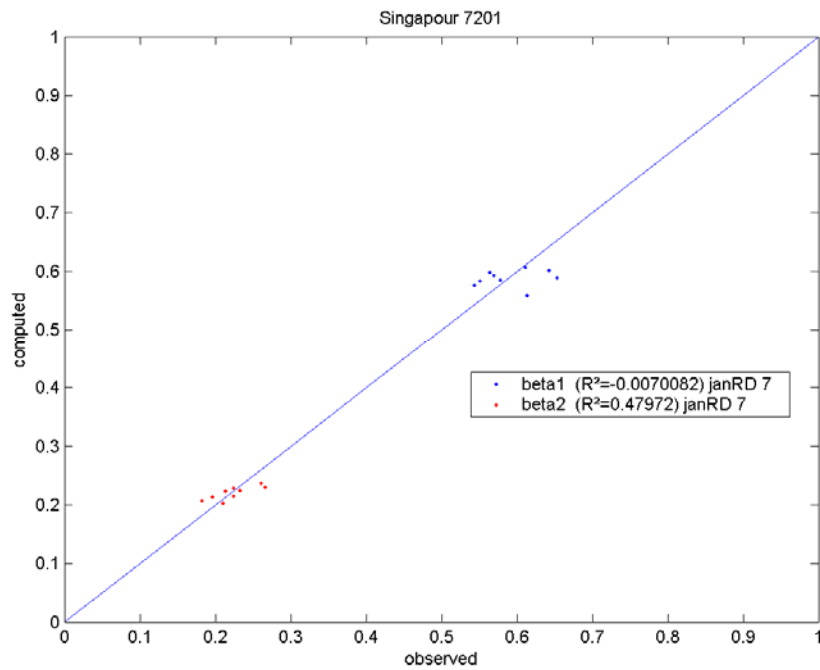
Figure 38: Results of the jackknife method with number of rainy days in January as rainfall parameters for partially gauged site.

4.4.3. Estimation of scaling slopes for un-gauged stations

	obs	com	AM	obs	com	wRD	Obs	com	MayRD	obs	com	OctRD
Ama Keng	111.6	127.2	13.98%	49.5	48.3	-2.31%	16.1	16.9	4.70%	18.2	18.0	-0.68%
Changi	145.9	134.0	-8.14%	31.3	43.5	38.73%	13.3	15.3	15.26%	15.3	15.9	4.11%
Jurond Ind	125.2	125.5	0.30%	35.6	47.6	33.85%	14.4	16.4	13.51%	16.8	17.4	3.80%
Macritche	125.3	130.6	4.27%	45.7	43.6	-4.57%	15.7	15.6	-0.58%	17.2	16.4	-4.83%
Paya Lebar	140.3	133.0	-5.21%	41.9	41.1	-1.95%	14.5	15.4	5.69%	15.1	16.4	8.97%
Seletar	130.9	131.1	0.13%	44.2	44.1	-0.19%	16.9	15.6	-7.36%	16.7	16.5	-0.82%
Spore Orchad	127.0	126.4	-0.48%	49.8	44.7	-10.15%	18.0	15.9	-11.61%	17.6	17.1	-2.99%
St James	130.8	128.1	-2.10%	43.1	43.5	0.79%	13.8	15.7	13.62%	14.7	16.9	14.98%
Tengah	127.0	116.4	-8.35%	50.0	47.1	-5.67%	17.2	16.0	-7.06%	18.4	17.8	-3.43%

	obs	comp	aRD	obs	comp	JanRD	Obs	comp	JunRD	obs	comp	NovRD
Ama Keng	189.8	193.1	1.78%	15.8	15.9	0.66%	13.6	13.7	1.01%	20.6	20.9	1.38%
Changi	150.4	176.9	17.65%	12.4	13.6	10.23%	13.0	13.3	1.76%	19.0	20.1	5.88%
Jurond Ind	159.1	187.7	17.95%	15.8	15.3	-3.19%	13.2	13.6	3.31%	19.8	20.5	3.50%
Macritche	180.5	176.9	-1.97%	14.5	14.4	-1.02%	14.0	13.3	-4.43%	20.7	20.0	-3.76%
Paya Lebar	173.3	172.4	-0.54%	12.7	13.9	9.26%	12.9	13.5	4.94%	19.9	19.9	-0.04%
Seletar	183.4	178.8	-2.49%	13.7	14.3	4.24%	13.9	13.5	-3.38%	20.3	20.3	-0.13%
Spore Orchad	196.5	180.8	-7.98%	15.8	14.9	-5.69%	14.0	13.6	-3.34%	21.0	20.4	-3.25%
St James	161.3	177.9	10.30%	13.9	14.7	5.48%	12.5	13.6	9.15%	18.2	20.4	11.85%
Tengah	198.1	184.9	-6.65%	16.1	15.6	-3.22%	13.7	13.5	-1.49%	21.1	20.5	-2.92%

	obs	com	sprRD	obs	com	FebRD	Obs	com	JulRD	obs	com	DecRD
Ama Keng	49.4	51.5	4.31%	13.3	13.3	-0.23%	13.4	13.5	0.74%	20.4	20.1	-1.38%
Changi	36.0	44.1	22.81%	9.7	11.1	14.89%	12.8	13.2	2.83%	19.3	19.2	-0.51%
Jurond Ind	41.9	48.8	16.61%	12.6	12.7	1.15%	12.6	13.4	6.53%	18.8	19.9	5.88%
Macritche	44.9	45.2	0.68%	11.9	11.8	-0.88%	13.6	13.2	-3.39%	19.3	19.3	-0.01%
Paya Lebar	42.1	43.4	3.06%	10.2	11.3	10.88%	13.0	13.3	2.90%	19.0	19.3	1.28%
Seletar	47.5	45.2	-4.83%	11.5	11.8	2.58%	13.9	13.3	-4.68%	19.0	19.5	2.52%
Spore Orchad	51.9	46.6	-10.21%	13.5	12.2	-9.64%	13.8	13.4	-3.31%	20.5	19.5	-5.01%
St James	39.3	45.4	15.44%	10.9	12.1	10.24%	12.1	13.4	10.03%	18.3	19.4	6.29%
Tengah	53.3	48.1	-9.72%	13.5	13.0	-3.59%	13.6	13.3	-2.03%	20.3	20.1	-1.21%

	obs	com	sumRD	obs	com	MarRD	Obs	comp	AugRD
Ama Keng	40.9	41.6	1.58%	16.1	15.9	-0.79%	14.0	14.3	2.61%
Changi	39.1	40.8	4.30%	12.6	13.9	10.38%	13.8	14.3	3.61%
Jurond Ind	40.2	41.4	2.89%	15.2	15.3	0.75%	13.8	14.3	4.22%
Macritche	42.0	40.9	-2.60%	14.8	14.3	-3.82%	14.4	14.4	-0.42%
Paya Lebar	40.0	41.2	2.91%	13.2	14.0	6.43%	14.1	14.4	2.04%
Seletar	43.1	41.2	-4.40%	14.2	14.5	1.65%	15.2	14.4	-5.01%
Spore Orchad	43.5	41.3	-5.18%	16.0	14.9	-6.48%	15.7	14.3	-8.95%
St James	37.7	41.4	9.81%	12.3	14.8	20.92%	13.1	14.4	9.54%
Tengah	41.6	41.0	-1.34%	16.2	15.7	-3.04%	14.3	14.1	-1.13%

	obs	comp	falRD	obs	comp	AprRD	Obs	comp	SepRD
Ama Keng	53.7	53.4	-0.69%	18.8	18.3	-2.68%	14.9	14.9	-0.27%
Changi	43.3	50.5	16.73%	14.9	16.1	7.83%	14.2	14.8	4.23%
Jurond Ind	44.8	52.8	17.96%	16.2	17.7	9.41%	14.2	14.9	5.25%
Macritche	53.0	50.1	-5.49%	16.6	16.6	-0.33%	15.1	14.7	-2.24%
Paya Lebar	49.7	49.3	-0.97%	15.3	16.4	7.09%	14.7	14.6	-0.66%
Seletar	51.6	51.1	-1.01%	17.2	16.6	-3.02%	14.6	15.0	2.67%
Spore Orchad	54.9	51.2	-6.80%	18.6	17.2	-7.66%	16.3	14.7	-9.62%
St James	46.7	50.8	8.85%	14.4	16.9	17.33%	13.7	14.9	8.57%
Tengah	54.4	52.3	-3.75%	18.7	18.2	-2.77%	14.9	14.9	0.30%

Table 12: Performance of the parameter estimation method (com=computed values and obs=observed values, the percentage being the difference between these values)

The proposed formula (Equation 24) for estimating rainfall parameters at an ungaged site gives results comparable to the observed values (Table 12). The stations with large discrepancies (Changi and Jurong Industrial Waterworks) are the ones with a large distance between them. In addition, their geographical situations near the coast of the island could explain these discrepancies as well since they have fewer neighbours with similar coastal effects, they have lower probability of having other stations with similar hydrologic features. Nevertheless, even theses estimates are fairly similar with the observed values.

On the basis of these good estimates, the slope of the second scaling regime is fairly well predicted at ungaged stations when the linear regression is based on the number of rainy days either in January or in February (Table 13 and Figure 39). However, the method is not able to do better than a random process to evaluate β_1 ($R^2 < 0$). Hence, the information on the number of rainy days in January or February is enough to extrapolate the scaling behavior of extreme precipitations at specific sites for duration in the order of hours, but not for shorter durations.

	Beta1	beta2
daily AM	-0.12	0.31
annual	-0.30	-0.07
January	-0.01	0.48
February	-0.08	0.39
March	-0.19	0.21
April	-0.31	0.10
May	-0.34	-0.09
June	-0.32	-0.20
July	-0.35	-0.26
August	-0.29	-0.25
September	-0.26	-0.27
October	-0.22	0.21
November	-0.28	-0.15
December	-0.32	-0.16

Table 13: Performance criterion (R²) of the jackknife method for un-gauged stations.
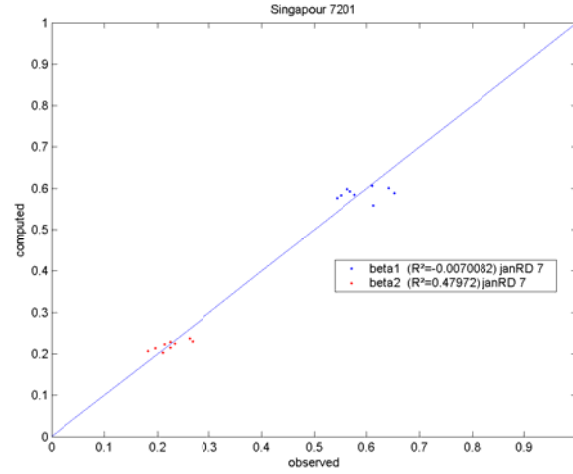
Figure 39: Results of the Jacknife method based on the number of rainy days in January for the 9 stations

4.5. Discussion

The present study aims at investigating the relationships between the scaling slopes and some rainfall parameters using a regional analysis. Results of this study have indicated that it is possible to estimate fairly well the rainfall scaling slopes based on information from surrounding stations as long as the site of interest has some information regarding the rainfall parameters. If there is no local information, only the slope of the temporal downscaling for longer durations (over than 45 minutes) can be reasonably estimated. However, in order to improve the estimation of the scaling functions for location with limited or without rainfall records further studies are needed to consider other nonlinear estimation methods or to find other rainfall parameters (see, for instance, Yu et al., 2004) that could provide a stronger relation with the scaling slopes.

5. Conclusions

The main objective of this study was to propose a method for estimating the IDF relations for gaged, partially-gaged, and ungaged sites for current and future climates. The proposed method was based on the combination of the spatial statistical downscaling SDSM technique and the temporal scaling GEV distribution. The feasibility of the temporal downscaling of the GEV distribution parameters was tested using observed AMP for 8 sub-daily durations for a station located in Quebec, Canada.

For the gaged sites, the performance of the proposed method has been tested using available extreme rainfall data at Dorval Airport, NCEP re-analysis data, and climate simulations from HadCM3 and CGCM2. Results of this evaluation have indicated the feasibility of the proposed procedure for deriving the IDF curves for both current and future climates. In addition, on the basis of the estimated IDF relations, the impacts of climate change on the urban design storms as well as on urban runoff properties can be successfully assessed. Finally, results of this study have indicated the high uncertainty of the different GCMs considered.

For the cases of partially-gaged and ungaged sites, a regional estimation has been proposed to estimate the rainfall scaling functions at these sites based on rainfall parameters from surrounding stations. Results of an illustrative application using available extreme rainfall data from nine stations in Singapore have indicated the feasibility of the proposed procedure. More specifically, it was found that the scaling function slopes exhibit significant correlations with the number of rainy days during some specific months (e.g., January and February during the monsoon season for Singapore); consequently, based on the number of rainy days, the scaling behaviour of extreme rainfall processes at a partially-gaged or ungaged site could be approximated and the IDF curves could be estimated.

51

Bibliography

Arisz, H. and Burrell, B.C. (2006) Urban Drainage Infrastructure Planning and Design Considering Climate Change, EIC Climate Change Technology 10-12 May 2006 pp 1-9.

Aronica, G.T. and Freni, G. (2005) Estimation of sub-hourly DDF curves using scaling properties of hourly and sub-hourly data at partially gauged site. Atmospheric Research 77(1-4), 114-123.

Burlando, P. and Rosso, R. (1996) Scaling and multiscaling models of depth-duration-frequency curves for storm precipitation. Journal of Hydrology 187(1-2), 45-64.

Chia, L.S., and Foong, S.F.(1991), Climate and Weather in L.S. Chia, A. Rahman, D.B.H. Tay, The Biophysical Environment of Singapore, Singapore University Press, Singapore, pp 13-49.

Denault, C., Millar, R.G. and Lence, B.J. (2002) Climate Change and Drainage Infrastructure Capacity in an Urban Catchment, Proceeding of the Annual Conference of the Canadian Society for Civil Engineering, Montréal, Québec, Canada.

Desbordes, M. 1978. Urban runoff and design storm modellin. In Urban storm drainage. Proceedings of the International Conference on Urban Storm Drainage, University Southampton, England, April 1978.Pentech Press, London, pp 352-361.

Flato, G.M. and Boer, G.J. (2001) Warming Asymmetry in Climate Change Simulations. Geophysical Research Letters 28(1), 195-198

Huber, W.C. and Dickinson, R.E. (1988) Stormwater management model user's manual, version 4. , Environmental Protection Agency, Athens, GA.

IPCC (2007) Climate Change (2007) Synthesis Report. Contribution of Working Groups I, II and III to the Fourth Assessment Report of the Intergovernmental Panel on Climate Change. Core Writing Team, Pachauri, R.K. and Reisinger, A. (eds), IPCC, Geneva, Switzerland.

Johns, T.C., Gregory, J.M., Ingram, W.J., Johnson, C.E., Jones, A., Lowe, J.A., Mitchell, J.F.B., Roberts, D.L., Sexton, D.M.H., Stevenson, D.S., Tett, S.F.B., Woodage, M.J. (2003) Anthropogenic climate change for 1860to 2100 simulated with the HadCM3 model under updated emissions scenarios. Climate Dynamics 20, 583-312.

Mailhot, A., Duchesne, S., Caya, D. and Talbot, G. (2007a) Assessment of future change in intensity-duration-frequency (IDF) curves for southern Quebec using the Canadian regional climate model (CRCM). Journal of Hydrology 347(1-2), 197-210.

Marsalek, J. and Watt, W.E. (1984) Design Storms for Urban Drainage Design. Canadian Journal of Civil Engineering 11(3), 574-584.

Menabde, M., Seed, A. and Pegram, G. (1999) A simple scaling model for extreme rainfall. Water Resources Research 35(1), 335-339.

Nakicenovic, N., Alcamo, J., Davis, G., de Vries, B., Fenhann, J., Gaffin, S., Gregory, K., Grubler, A., Jung, T.Y., Kram, T., La Rovere, E.L., Michaelis, L., Mori, S., Morita, T., Pepper, W., Pitcher, H.M., Price, L., Riahi, K., Roehrl, A., Rogner, H.H., Sankovski, A., Schlesinger, M., Shukla, P., Smith, S.J., Swart, R., van Rooijen, S., Victor, N., Dadi, Z. (2000) Special Report on Emissions Scenarios: A Special Report of Working Group III of the Intergovernmental Panel on Climate Change, Cambridge University Press, Cambridge, U.K., 599 pp.

Nguyen, V.T.V., Nguyen, T.D. and Ashkar, F. (2002) Regional frequency analysis of extreme rainfalls. Water Science and Technology 45(2), 75-81.

Nguyen, V.T.V., Nguyen, T.D. and Cung, A. (2006) A statistical downscaling approach to development of intensity-duration-frequency relations in consideration of climate variability and change, Proceeding in 7th International Workshop on precipitation in urban areas, Saint Moritz, Switzerland.

Nguyen, V.T.V., Nguyen, T.D. and Wang, H. (1998) Regional estimation of short duration rainfall extremes. Water Science and Technology 37(11), 15-19.

Nhat, L.M., Tachikawa, Y., Sayama, T. and Takara, K. (2006) Derivation of Rainfall Intensity-Duration-Frequency Relationships for Short-Duration Rainfall from Daily Data. IHP Technical Documents in Hydrology 6, 89-96.

Over, T.M. and Gupta, V.K. (1994) Statistical-Analysis of Mesoscale Rainfall - Dependence of a Random Cascade Generator on Large-Scale Forcing. Journal of Applied Meteorology 33(12), 1526-1542.

Peyron, N. (2001) Design Storms for Urban Runoff Estimation. Project Report, McGill University, Montréal, Canada.

Peyron, N., Nguyen, V.T.V. and Rivard, G. (2005) Un modele optimal de pluie de projet pour la conception des reseaux de drainage urbain. Annales du batiment et des travaux publics, 35-42.

Redano, A. and Lorente, J. (1993) Modeling the Spatial and Temporal Distribution of Rainfall Intensity at Local Scale. Theoretical and Applied Climatology 47(1), 25-32.

Ruth, M., Donaghy, K. and Kirshen, P.H. (2006) Regional climate change and variability: impacts and responses, Edward Elgar, Cheltenham, UK; Northampton, MA.

Semadeni-Davies, A. (2004) Urban Water Management vs. Climate Change: Impact on Cold Region Waste Water Inflows. Climatic Change 64(1-2), 103-126.

Watt, W.E., Chow, K.C.A., Hogg, W.D. and Lathem, K.W. (1986) A 1-H Urban Design Storm for Canada. Canadian Journal of Civil Engineering 13(3), 293-300.

Watt, W.E., Waters, D. and McLean, R. (2003) Climate Change and Urban Stormwater Infrastructure in Canada: Context and Case Studies. Study, T.-N.R. (ed), p. 27, Meteorological Service of Canada, Waterloo, Ontario, Canada.

Wilby, R.L., Dawson, C.W. and Barrow, E.M. (2002) SDSM - a decision support tool for the assessment of regional climate change impacts. Environmental Modelling & Software 17(2), 147-159.

Yu, P.S., Yang, T.C. and Lin, C.S. (2004) Regional rainfall intensity formulas based on scaling property of rainfall. Journal of Hydrology 295(1-4), 108-123.

-

APPENDICES

A – Analysis of the consistency between the different sets of data

-

year	5-min	10-min	15-min	30-min	1-h	2-h	6-h	12-h
1961	-12.7%	8.8%	9.6%	-7.6%	-10.2%	-15.2%	-13.3%	-8.9%
1962	49.5%	-10.3%	-5.7%	-2.0%	-1.7%	0.0%	2.8%	-3.1%
1963	-13.4%	-2.0%	-1.6%	-5.5%	-6.5%	-6.2%	3.1%	23.7%
1964	35.3%	38.0%	33.2%	61.7%	29.3%	0.5%	0.5%	26.7%
1965	-4.5%	-5.1%	-1.8%	-0.1%	-5.2%	-2.3%	30.7%	89.4%
1966	0.0%	-2.6%	-5.5%	-3.5%	-3.6%	-3.2%	-2.0%	0.6%
1967	12.2%	10.2%	3.6%	-3.8%	-3.8%	-3.8%	-3.8%	20.7%
1968	0.0%	-2.5%	5.4%	1.1%	1.0%	1.0%	2.3%	17.6%
1969	20.8%	-0.2%	13.7%	12.5%	14.5%	14.5%	14.5%	14.5%
1970	634.4%	710.5%	557.6%	441.1%	395.5%	533.1%	478.2%	478.2%
1971	4.6%	5.0%	4.3%	13.5%	4.1%	6.7%	12.8%	12.8%
1972	116.0%	52.8%	46.6%	17.1%	6.9%	9.6%	8.8%	9.9%
1973	36.4%	7.1%	16.9%	1.6%	20.1%	19.2%	19.2%	19.2%
1974	1.7%	-5.5%	6.1%	11.6%	14.0%	26.3%	17.2%	28.9%
1975	31.8%	27.0%	9.4%	-6.1%	24.0%	21.4%	23.3%	88.6%
1976	24.1%	19.1%	21.1%	4.7%	3.1%	9.7%	19.1%	51.5%
1977	33.3%	3.0%	2.3%	10.0%	12.4%	7.7%	-23.1%	-21.5%
1978	18.0%	19.0%	6.3%	5.6%	0.8%	-20.3%	21.1%	22.4%
1979	17.5%	12.5%	5.0%	22.5%	31.5%	29.9%	88.7%	161.2%
1980	8.8%	-14.4%	-12.2%	-12.8%	-14.5%	-4.5%	-3.1%	-3.2%
1981	4.3%	-0.8%	-1.2%	3.3%	3.4%	4.0%	5.0%	14.2%
1982	-2.5%	7.4%	15.9%	9.3%	15.5%	16.5%	14.9%	14.9%
1983	-14.3%	30.4%	18.6%	-12.6%	-6.0%	-10.4%	-41.2%	-6.8%
1984	16.1%	-10.0%	-11.0%	7.0%	-3.6%	-5.0%	61.1%	19.6%
1985	370.0%	200.0%	136.7%	55.8%	12.5%	27.3%	63.6%	80.6%
1986	-6.3%	-10.7%	-7.5%	4.0%	5.1%	16.7%	3.2%	5.7%
1987	13.6%	2.2%	-3.6%	-5.4%	0.7%	0.4%	-15.7%	-14.8%
1988	-19.2%	-26.1%	-15.7%	-15.7%	-15.8%	-15.6%	-14.4%	0.2%
1989	-7.1%	-2.3%	-1.1%	-11.2%	0.0%	0.0%	0.5%	8.9%
1990	2.0%	7.0%	3.3%	3.2%	2.8%	-2.8%	-3.1%	6.8%
1991	205.0%	155.0%	130.0%	130.0%	48.9%	26.7%	64.8%	89.0%
1992	13.6%	9.4%	0.8%	2.3%	24.7%	63.6%	8.3%	37.2%
1993	40.0%	9.0%	3.2%	4.4%	4.3%	6.4%	8.9%	6.1%
1994	113.9%	97.2%	57.8%	11.8%	11.6%	9.9%	3.5%	3.5%

-

Table 14: Relative difference between observed AMP and annual maximum precipitation depths computed from the available historical storms

B-Computation of GEV Quantile

Notations:

Notations:

p = $exceedance\ probability = P(X > X_\tau)$

X_τ = $quantile\ associated\ with\ the\ return\ period\ \tau$

F = $cumulative\ distribution\ function$

p = $1 - F(X_\tau)$

$$1 - p = exp\left\{-\left[1 - \frac{\kappa}{\alpha}(X_\tau - \xi)\right]^{\frac{1}{\kappa}}\right\}$$

$$\ln(1 - p) = -\left[1 - \frac{\kappa}{\alpha}(X_\tau - \xi)\right]^{\frac{1}{\kappa}}$$

$$1 - \frac{\kappa}{\alpha}(X_\tau - \xi) = [-\ln(1 - p)]^\kappa$$

$$(X_\tau - \xi) = \frac{\alpha}{\kappa}[1 - [-\ln(1 - p)]^\kappa]$$

$$X_\tau = \xi + \frac{\alpha}{\kappa}[1 - [-\ln(1 - p)]^\kappa] \text{Notations:}$$

C-Determination of the three GEV parameters from the 3 first NCM

We have

$$\mu_1 = \left(\xi + \frac{\alpha}{\kappa}\right) - \frac{\alpha}{\kappa}\Gamma(1+\kappa)$$

$$\mu_2 = \left(\xi + \frac{\alpha}{\kappa}\right)^2 + \left(\frac{\alpha}{\kappa}\right)^2 \Gamma(1+2\kappa) - 2\frac{\alpha}{\kappa}\left(\xi + \frac{\alpha}{\kappa}\right)\Gamma(1+\kappa)$$

$$\mu_3 = \left(\xi + \frac{\alpha}{\kappa}\right)^3 - \left(\frac{\alpha}{\kappa}\right)^3 \Gamma(1+3\kappa) + 3\left(\frac{\alpha}{\kappa}\right)^2\left(\xi + \frac{\alpha}{\kappa}\right)\Gamma(1+2\kappa)$$

$$- 3\left(\frac{\alpha}{\kappa}\right)\left(\xi + \frac{\alpha}{\kappa}\right)^2 \Gamma(1+\kappa)$$

Notations:

$$\boldsymbol{G_1} = \Gamma(1+\kappa)$$
$$\boldsymbol{G_2} = \Gamma(1+2\kappa)$$
$$\boldsymbol{G_3} = \Gamma(1+3\kappa)$$
$$\mathbf{B} = \mu_1{}^2 - \mu_2$$
$$\boldsymbol{C} = 2\mu_1{}^3 - 3\mu_1\mu_2 + \mu_3$$
$$\mathbf{D} = \boldsymbol{G_1}^2 - \boldsymbol{G_2}$$
$$\mathbf{E} = 2\boldsymbol{G_1}^3 - 3\boldsymbol{G_1}\boldsymbol{G_2} + \boldsymbol{G_3}$$

So, the NCM can be written as

$$\mu_1 = \left(\xi + \frac{\alpha}{\kappa}\right) - \frac{\alpha}{\kappa}G_1$$

$$\mu_2 = \left(\xi + \frac{\alpha}{\kappa}\right)^2 + \left(\frac{\alpha}{\kappa}\right)^2 G_2 - 2\frac{\alpha}{\kappa}\left(\xi + \frac{\alpha}{\kappa}\right)G_1$$

$$\mu_3 = \left(\xi + \frac{\alpha}{\kappa}\right)^3 - \left(\frac{\alpha}{\kappa}\right)^3 G_3 + 3\left(\frac{\alpha}{\kappa}\right)^2\left(\xi + \frac{\alpha}{\kappa}\right)G_2 - 3\left(\frac{\alpha}{\kappa}\right)\left(\xi + \frac{\alpha}{\kappa}\right)^2 G_1$$

Thus, we get

$$B = \left(\left(\xi + \frac{\alpha}{\kappa}\right) - \frac{\alpha}{\kappa}G_1\right)^2 - \left[\left(\xi + \frac{\alpha}{\kappa}\right)^2 - \left(\frac{\alpha}{\kappa}\right)^2 G_2 - 2\frac{\alpha}{\kappa}\left(\xi + \frac{\alpha}{\kappa}\right)G_1\right]$$

$$B = \left(\xi + \frac{\alpha}{\kappa}\right)^2 - 2\left(\xi + \frac{\alpha}{\kappa}\right)\frac{\alpha}{\kappa}G_1 + \left(\frac{\alpha}{\kappa}G_1\right)^2 - \left(\xi + \frac{\alpha}{\kappa}\right)^2 + \left(\frac{\alpha}{\kappa}\right)^2 G_2$$

$$+ 2\frac{\alpha}{\kappa}\left(\xi + \frac{\alpha}{\kappa}\right)G_1$$

$$B = \left(\frac{\alpha}{\kappa}\right)^2 \left(G_2 - G_1{}^2\right) + \left(\xi + \frac{\alpha}{\kappa}\right)^2 (1 - 1) + 2\left(\xi + \frac{\alpha}{\kappa}\right)\frac{\alpha}{\kappa}G_1(2 - 2)$$

$$B = \left(\frac{\alpha}{\kappa}\right)^2 D$$

$$\Rightarrow \alpha = \kappa \left(\frac{B}{D}\right)^{1/2}$$

And

$$C = 2\left(\left(\xi + \frac{\alpha}{\kappa}\right) - \frac{\alpha}{\kappa}G_1\right)^3$$

$$- 3\left(\left(\xi + \frac{\alpha}{\kappa}\right) - \frac{\alpha}{\kappa}G_1\right)\left(\left(\xi + \frac{\alpha}{\kappa}\right)^2 + \left(\frac{\alpha}{\kappa}\right)^2 G_2 - 2\frac{\alpha}{\kappa}\left(\xi + \frac{\alpha}{\kappa}\right)G_1\right)$$

$$+ \left(\xi + \frac{\alpha}{\kappa}\right)^3 - \left(\frac{\alpha}{\kappa}\right)^3 G_3 + 3\left(\frac{\alpha}{\kappa}\right)^2\left(\xi + \frac{\alpha}{\kappa}\right)G_2 - 3\left(\frac{\alpha}{\kappa}\right)\left(\xi + \frac{\alpha}{\kappa}\right)^2 G_1$$

$$C = \left(\xi + \frac{\alpha}{\kappa}\right)^3 (2 - 3 + 1) + \left(\xi + \frac{\alpha}{\kappa}\right)^2\left(\frac{\alpha}{\kappa}G_1\right)(2(-3) + 3 - 2(-3) - 3)$$

$$+ \left(\xi + \frac{\alpha}{\kappa}\right)\left(\frac{\alpha}{\kappa}\right)^2 (2(3)G_1 + 3(-2)G_1 - 3G_2 + 3G_2)$$

$$+ \left(\frac{\alpha}{\kappa}\right)^3 \left(-2G_1{}^3 + 3G_1G_2 - G_3\right)$$

$$C = \left(\frac{\alpha}{\kappa}\right)^3 (-E)$$

Hence we get these 3 independent equations to find the 3 parameters:

$$\alpha = \kappa \left(\frac{B}{D}\right)^{1/2}$$

$$\xi = \mu_1 + \frac{\alpha}{\kappa}(G_1 - 1)$$

$$C + \left(\frac{B}{D}\right)^{3/2} E = 0$$
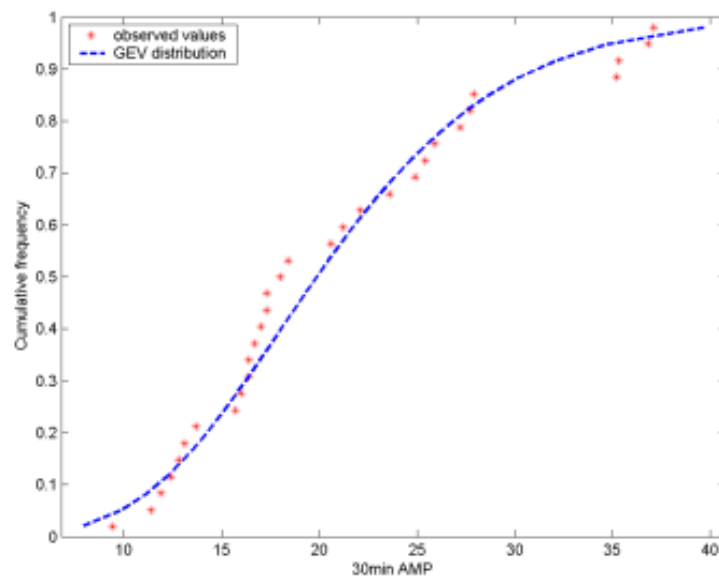
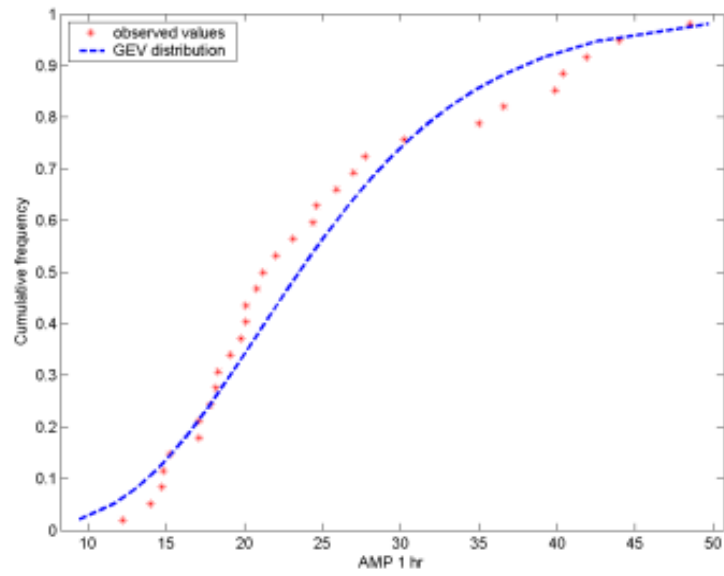# D- Quantile Plots of the AMP for the baseline period
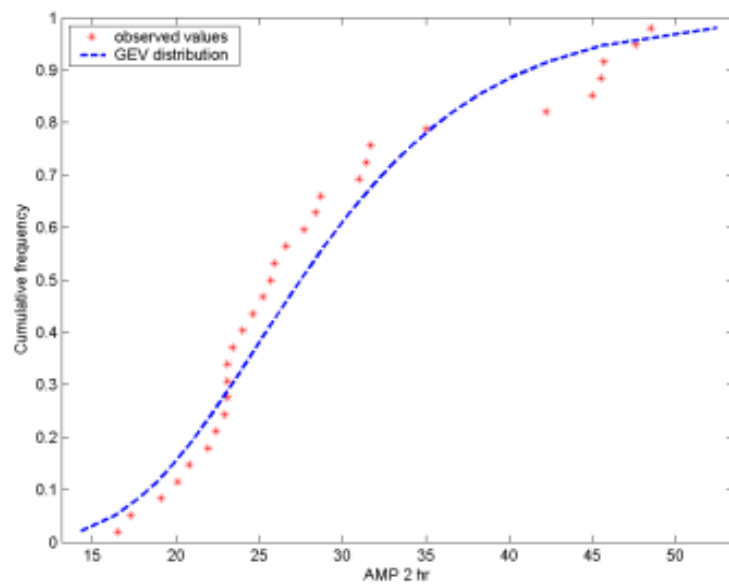
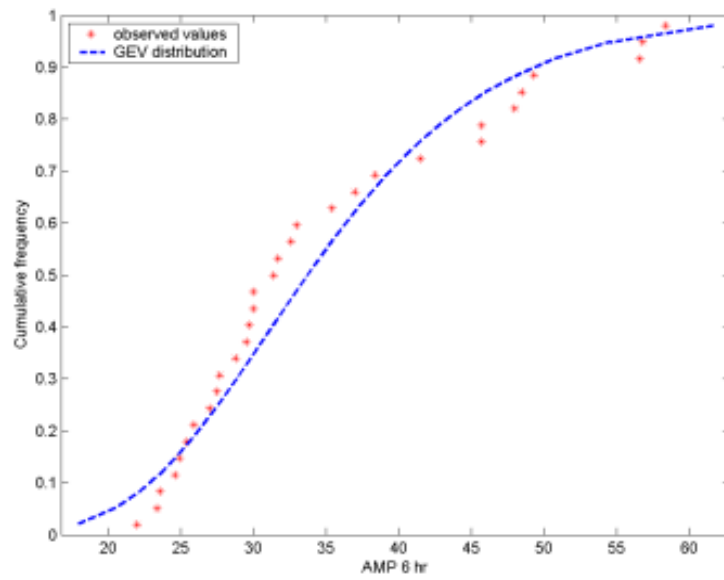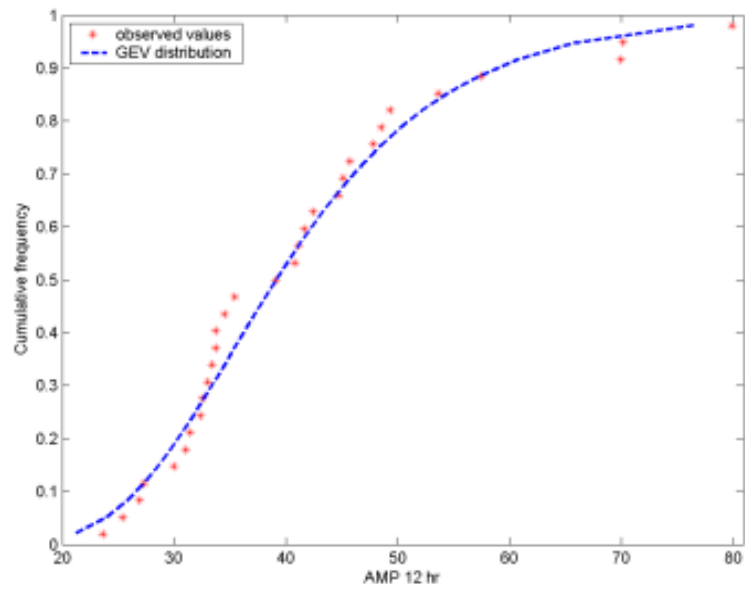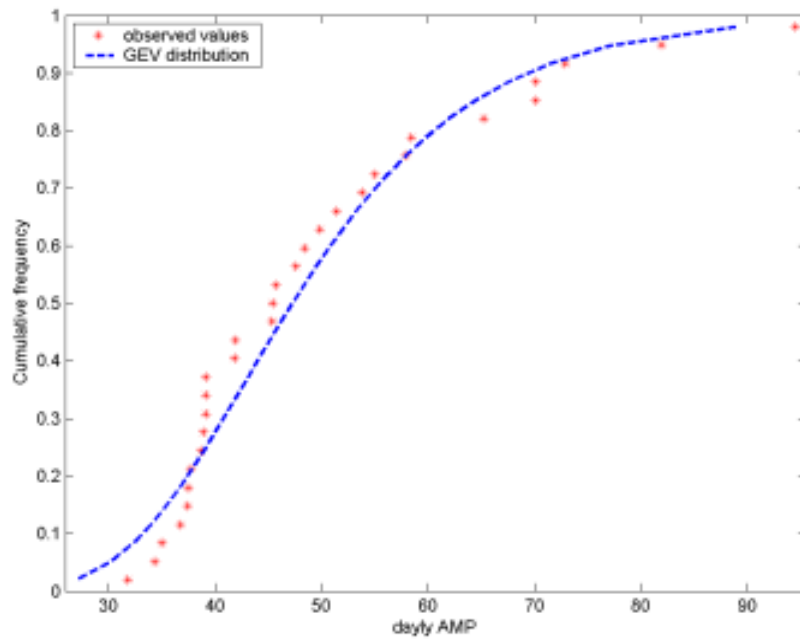5 minutes
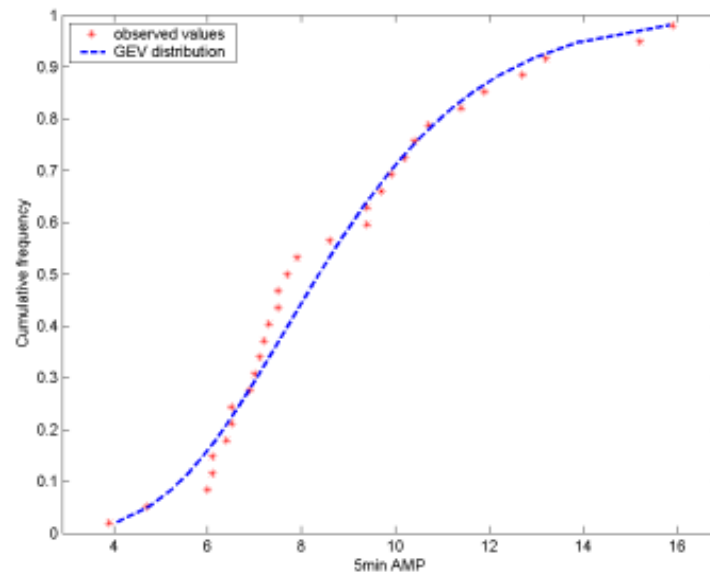
10 minutes
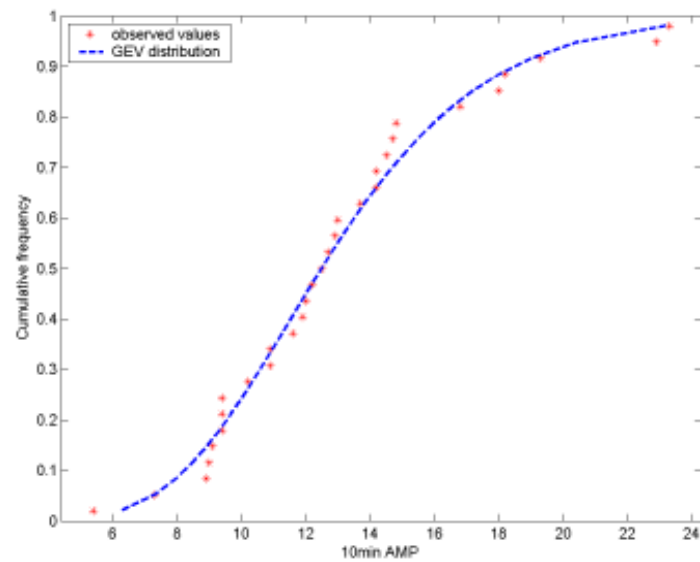
15 minutes
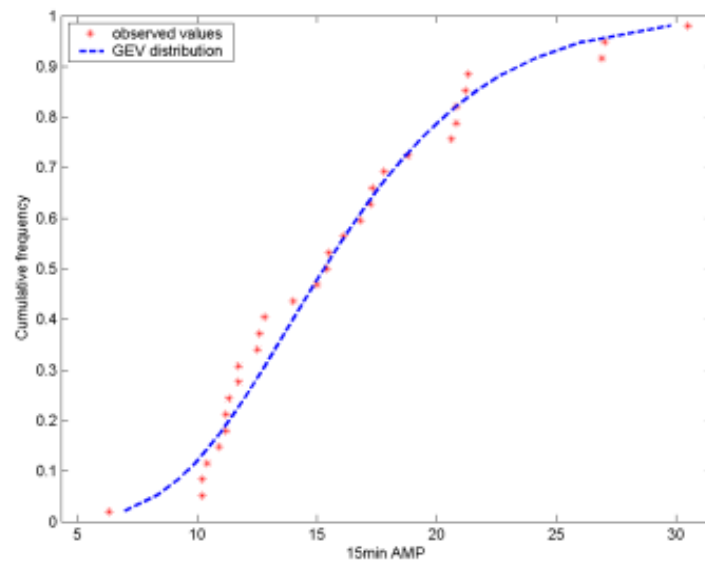
30 minutes

1 hour

2 hours

6 hours
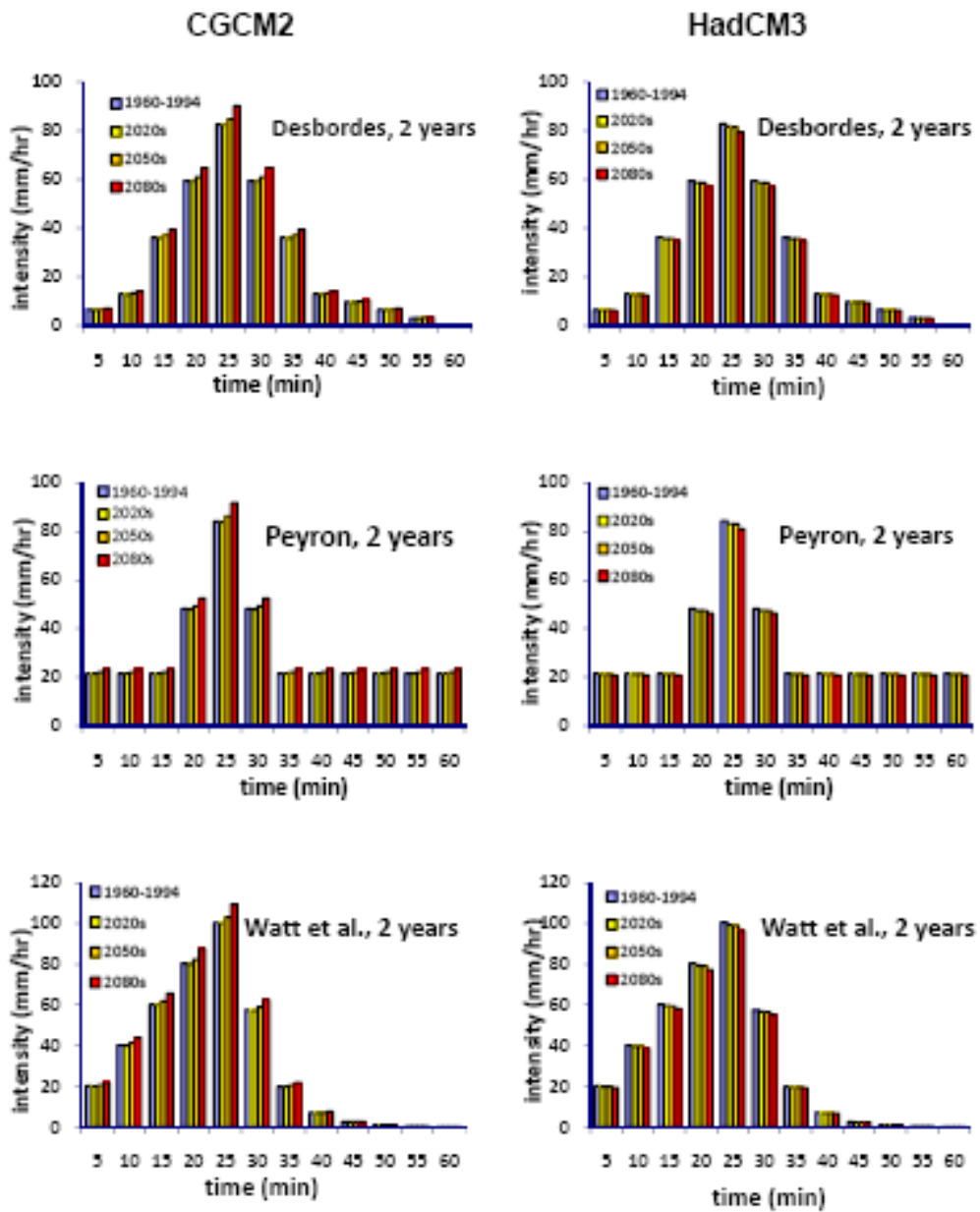

12 hours

1 day

E- Evolution of the design storms

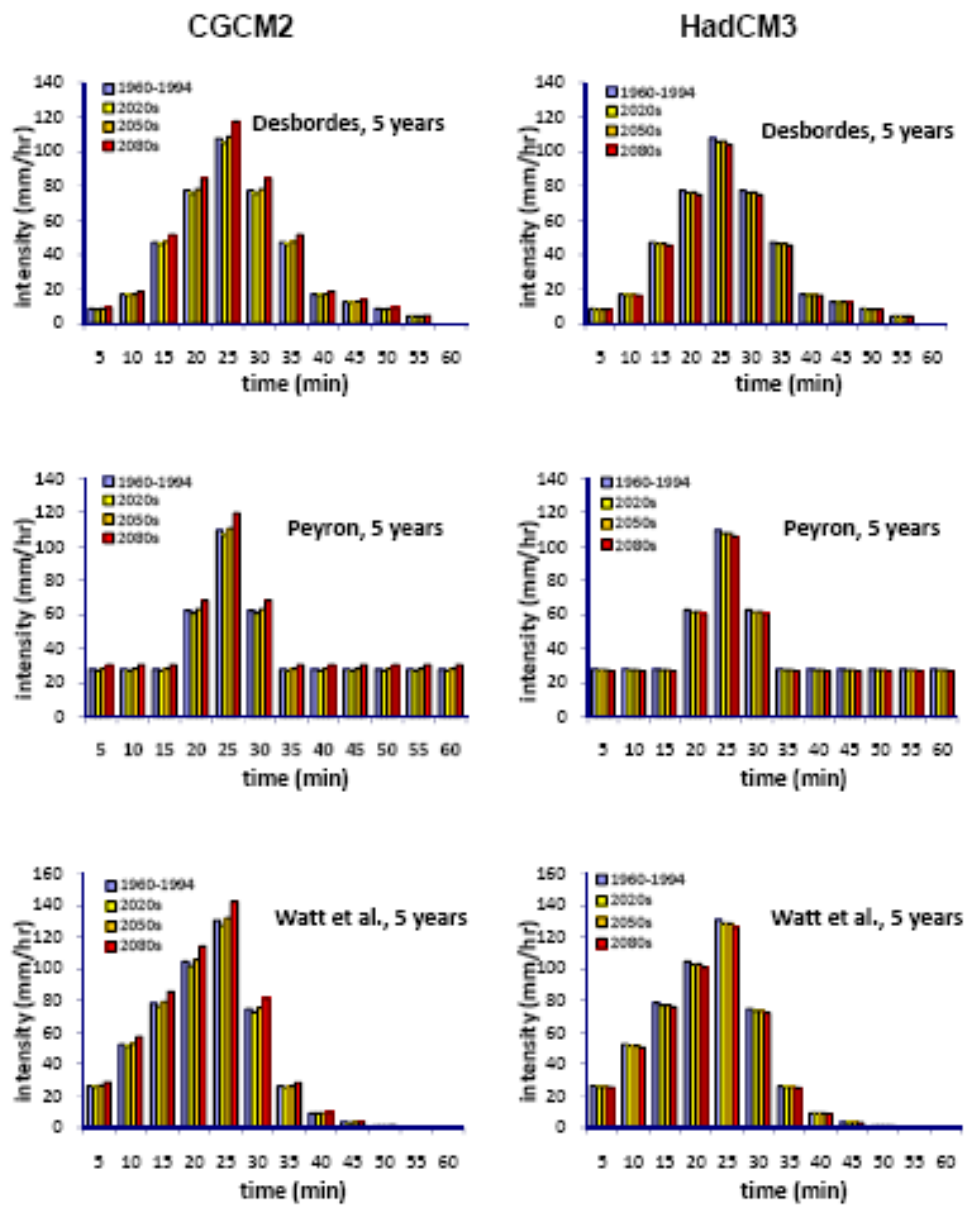Figure 40: Design Storms for the 4 periods for the 2-year return period

Figure 41: Design storms for the 4 periods for the 5-year return period
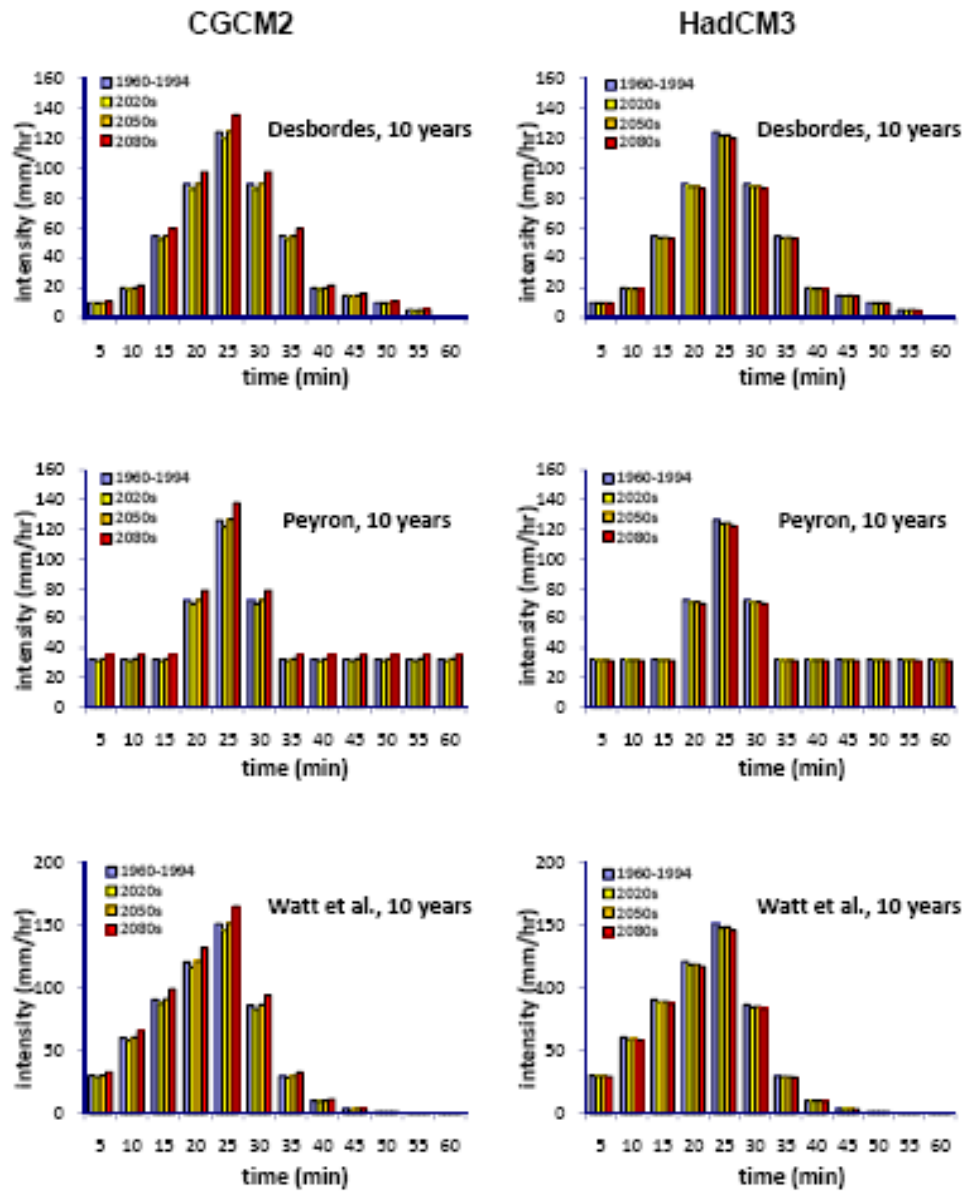
Figure 42: Design storms for the 4 periods for the 10-year return period
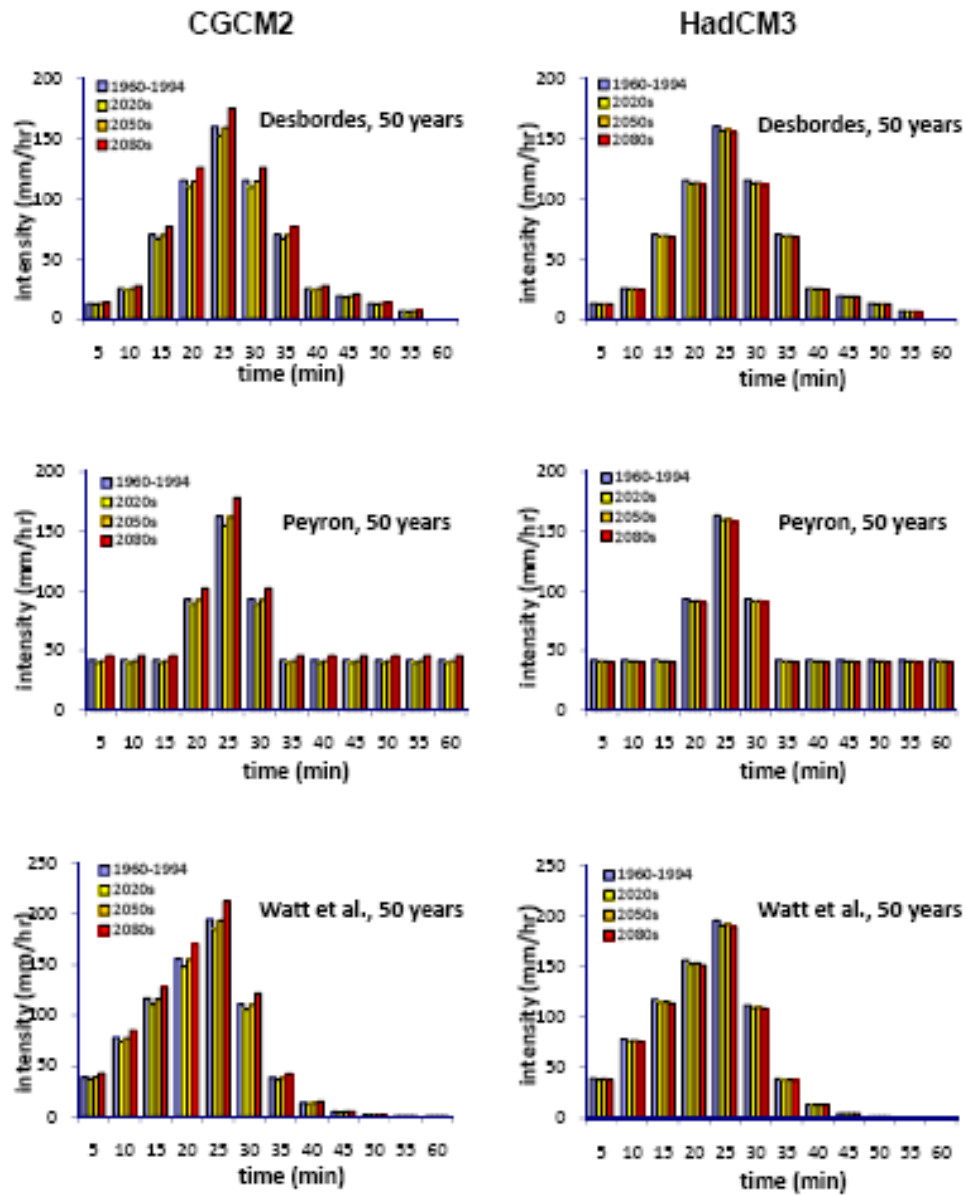
Figure 43: Design storms for the 4 periods for the 50-year return period

F- Evolution of the runoff values in the different watershed configurations
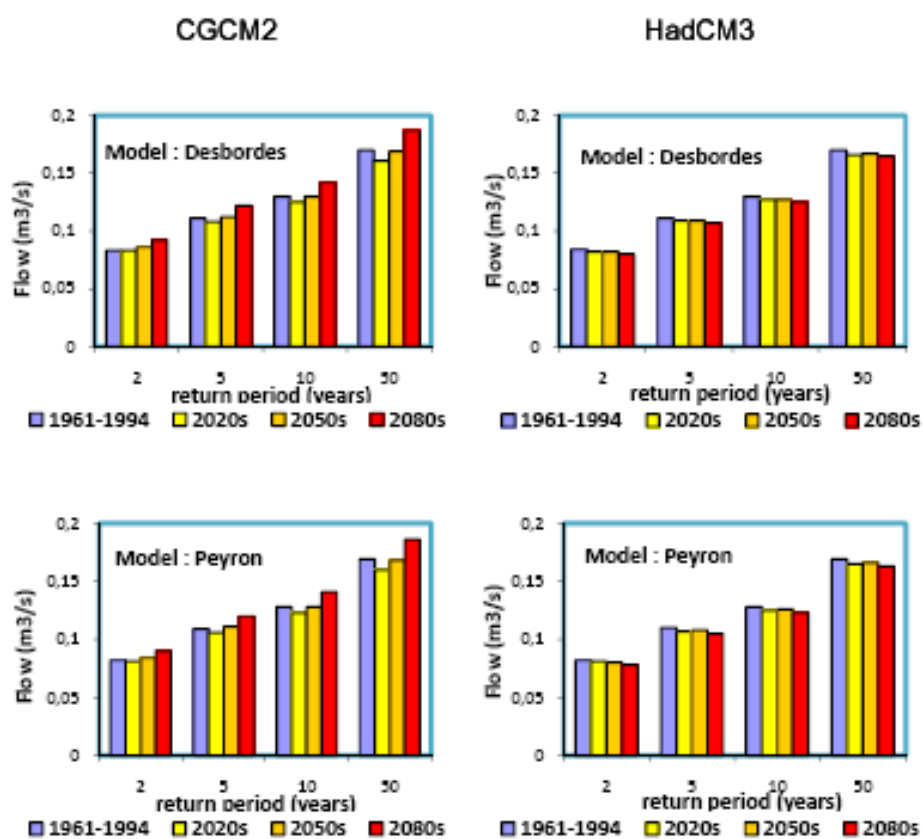
Figure 44: Evolution of the runoff peak flows (Rect, 100%, 0.4ha)
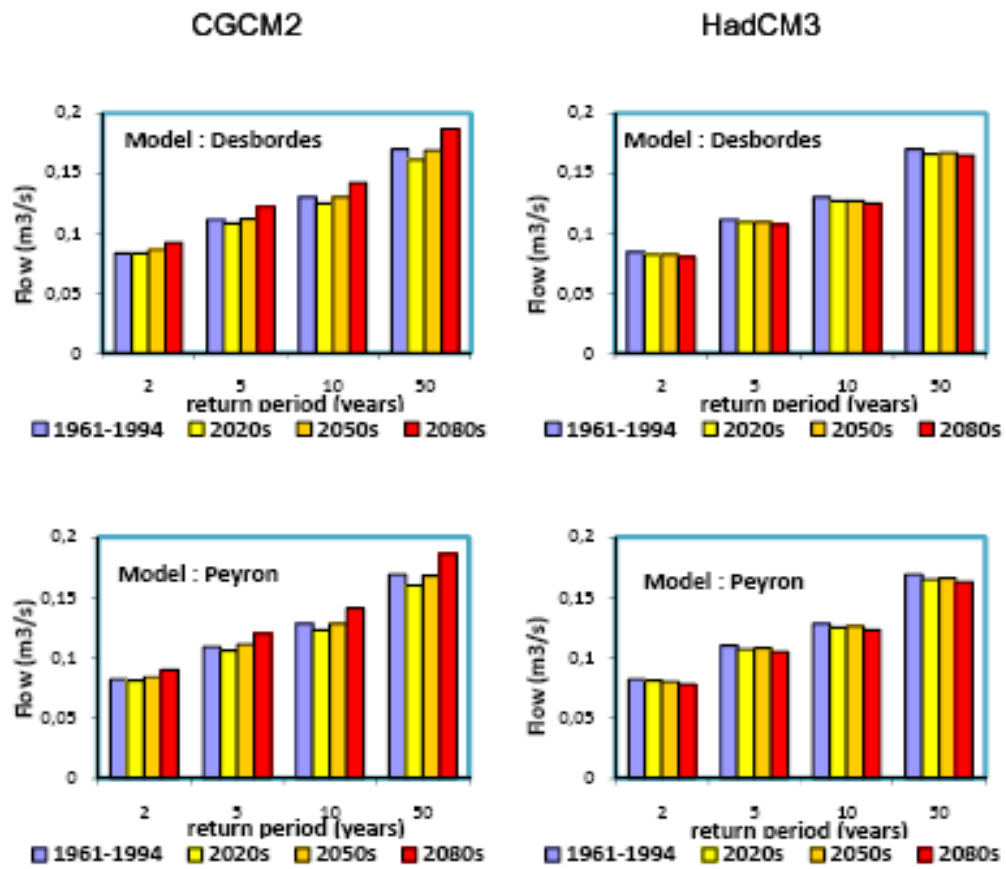
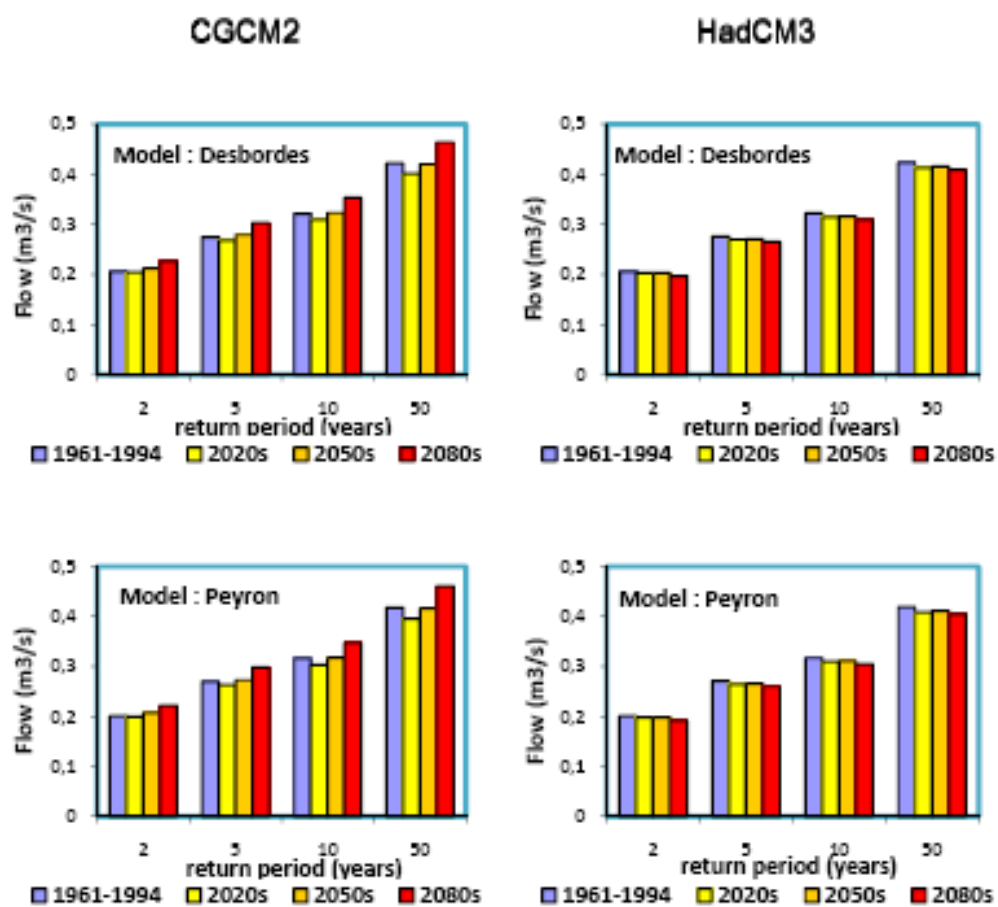**Figure 45: Evolution of the runoff peak flows (Rect, 100%, 2 ha)**

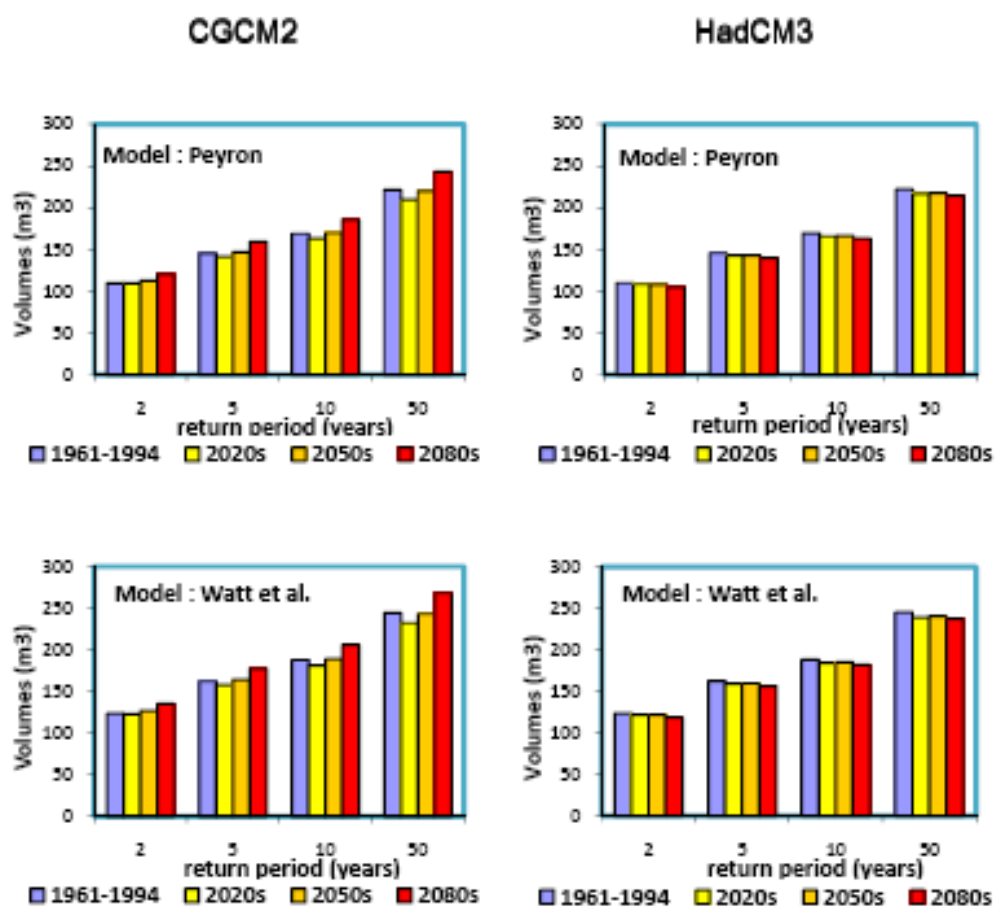**Figure 46: Evolution of the runoff peak flows (Square, 65%, 10 ha)**

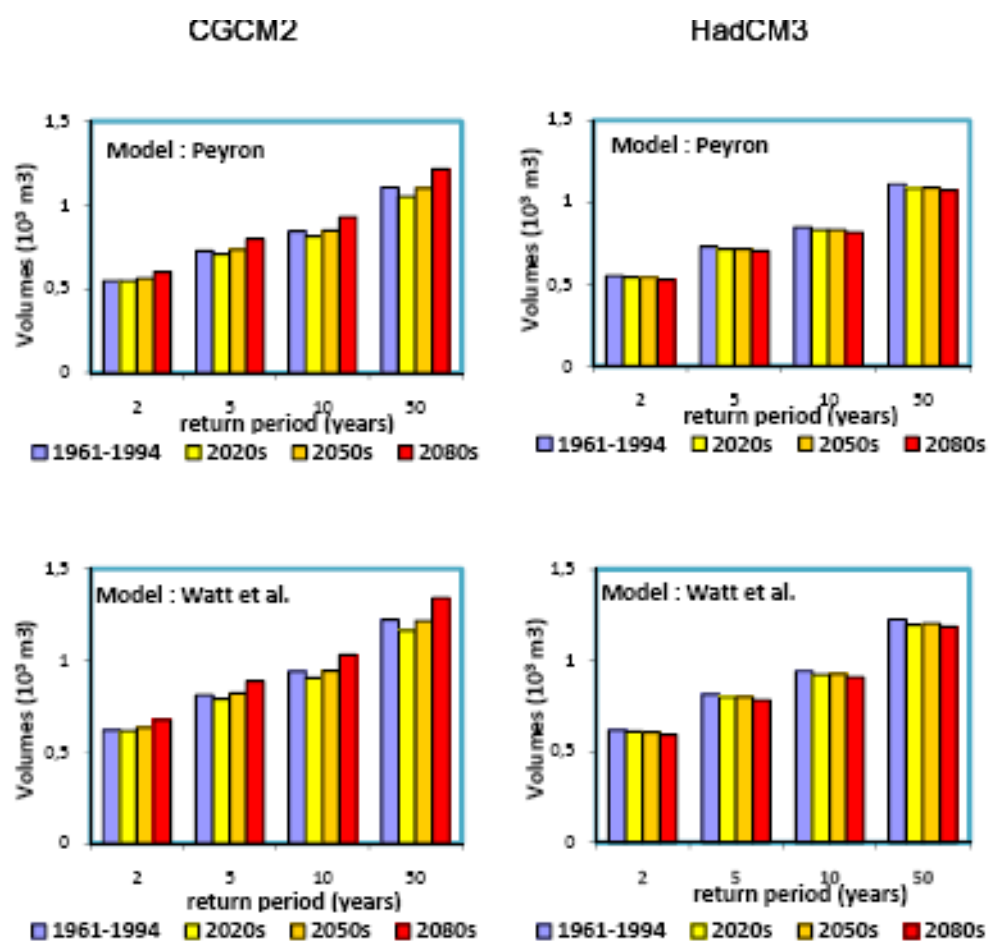**Figure 47: Evolution of the runoff volume (Rect, 100%, 0.4 ha)**

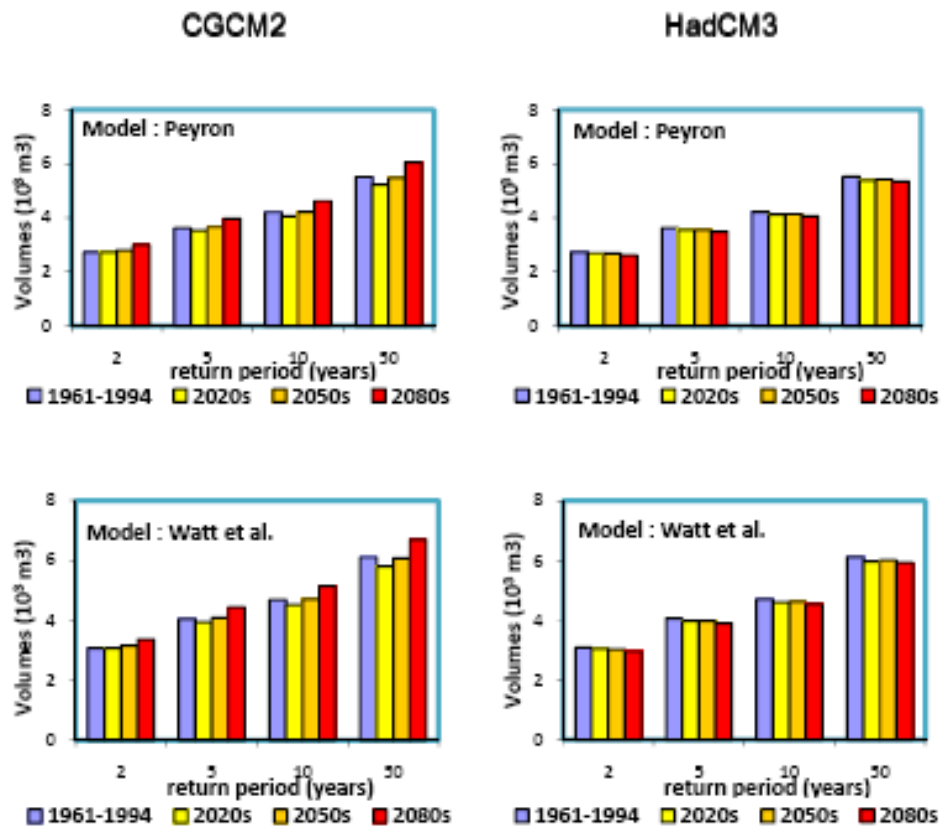**Figure 48: Evolution of the runoff volumes (Rect, 100%, 2ha)**

Figure 49: Evolution of the runoff volumes (Square, 65%, 10 ha)